GNC 2017 : 10th International ESA Conference on Guidance, Navigation & Control Systems
29 May - 2 June 2017, Salzburg, Austria
European Space Agency

IN-FLIGHT GUIDANCE, NAVIGATION, AND CONTROL PERFORMANCE RESULTS FOR THE GOES-16 SPACECRAFT

Jim Chapel[1], Devin Stancliffe[2], Tim Bevacqua[2], Stephen Winkler[2], Brian Clapp[2]
Tim Rood[3], Doug Freesland[4], Alan Reth[5], Derrick Early[5],
Tim Walsh[6], Alexander Krimchansky[7]

[1]Lockheed Martin Space Systems, Denver, CO, USA, +1-303-977-9462, jim.d.chapel@lmco.com
[2]Lockheed Martin Space Systems, Denver, CO, USA
[3]Advanced Solutions Inc., Littleton, CO, USA
[4]ACS Engineering, Columbia, MD, USA
[5]Chesapeake Aerospace, Grasonville, MD, USA
[6]NOAA/Goddard Space Flight Center, Greenbelt, MD, USA
[7]NASA/Goddard Space Flight Center, Greenbelt, MD, USA

ABSTRACT

The Geostationary Operational Environmental Satellite-R Series (GOES-R), which launched in November 2016, is the first of the next generation geostationary weather satellites. GOES-R provides 4 times the resolution, 5 times the observation rate, and 3 times the number of spectral bands for Earth observations compared with its predecessor spacecraft. Additionally, Earth-relative and Sun-relative pointing and pointing stability requirements are maintained throughout reaction wheel desaturation events and station keeping activities, allowing GOES-R to provide continuous Earth and sun observations. This paper reviews the pointing control, pointing stability, attitude knowledge, and orbit knowledge requirements necessary to realize the ambitious Image Navigation and Registration (INR) objectives of GOES-R. This paper presents a comparison between low-frequency on-orbit pointing results and simulation predictions for both the Earth Pointed Platform (EPP) and Sun Pointed Platform (SPP). Results indicate excellent agreement between simulation predictions and observed on-orbit performance, and compliance with pointing performance requirements. The EPP instrument suite includes 6 seismic accelerometers sampled at 2 KHz, allowing in-flight verification of jitter responses and comparison back to simulation predictions. This paper presents flight results of acceleration, shock response spectrum (SRS), and instrument line of sight responses for various operational scenarios and instrument observation modes. The results demonstrate the effectiveness of the dual-isolation approach employed on GOES-R. The spacecraft provides attitude and rate data to the primary Earth-observing instrument at 100 Hz, which are used to adjust instrument scanning. The data must meet accuracy and latency numbers defined by the Integrated Rate Error (IRE) requirements. This paper discusses the on-orbit IRE results, showing compliance to these requirements with margin. During the spacecraft checkout period, IRE disturbances were observed and subsequently attributed to thermal control of the Inertial Measurement Unit (IMU) mounting interface. Adjustments of IMU thermal control and the resulting improvements in IRE are presented. Orbit knowledge represents the final element of INR performance. Extremely accurate orbital position is achieved by GPS navigation at Geosynchronous Earth Orbit (GEO). On-orbit performance results are shown demonstrating compliance with the stringent orbit position accuracy requirements of GOES-R, including during station keeping activities and momentum desaturation events. As we show in this paper, the on-orbit performance of the GN&C design provides the necessary capabilities to achieve GOES-R mission objectives.

1. GOES-R MISSION OBJECTIVES

The GOES-R spacecraft launched November 19, 2016, and is the first of a new generation U.S. geostationary weather satellites. After achieving its operational configuration in geostationary orbit, GOES-R was subsequently renamed GOES-16. In this paper, “GOES-R” will be generally used when discussing the design of the spacecraft series, and “GOES-16” will be used when discussing flight data. The National Oceanic and

Atmospheric Administration (NOAA) and the National Aeronautics and Space Administration (NASA) manage the program cooperatively. The mission includes hosting both Earth-observing and space weather instruments, hosting a communication payload to deliver instrument data to the data processing centers, serving as a data collection platform, and providing search and rescue services. In this paper we provide an initial look at flight data from GOES-16, and we build upon design material previously provided in [1][2].

Relative to the current generation of GOES satellites, the GOES-R Advanced Baseline Imager (ABI), represents a dramatic increase in Earth weather observation capabilities. ABI provides 4 times the resolution, 5 times the observation rate, 100 times data rate and 3 times the number of spectral bands for Earth observations [3]. In addition to ABI, a newly-developed Earth-observing instrument is hosted by the spacecraft—Geostationary Lightning Mapper (GLM). GLM is a near-infrared optical transient detector, which can detect extremely brief changes in an optical scene, indicating the presence of lightning. The configuration of these instruments on the GOES-R EPP is shown in Fig. 1.

Both Earth-pointed instruments demand high spacecraft pointing and pointing stability performance to produce the desired data return. Unlike previous GOES spacecraft, performance requirements must be met during momentum unload events and station-keeping maneuvers. The GOES-R spacecraft is only allocated 120 minutes per year where the pointing and stability requirements can be exceeded [4][5]. This "operate-through" capability will provide unprecedented observation availability to the user community.

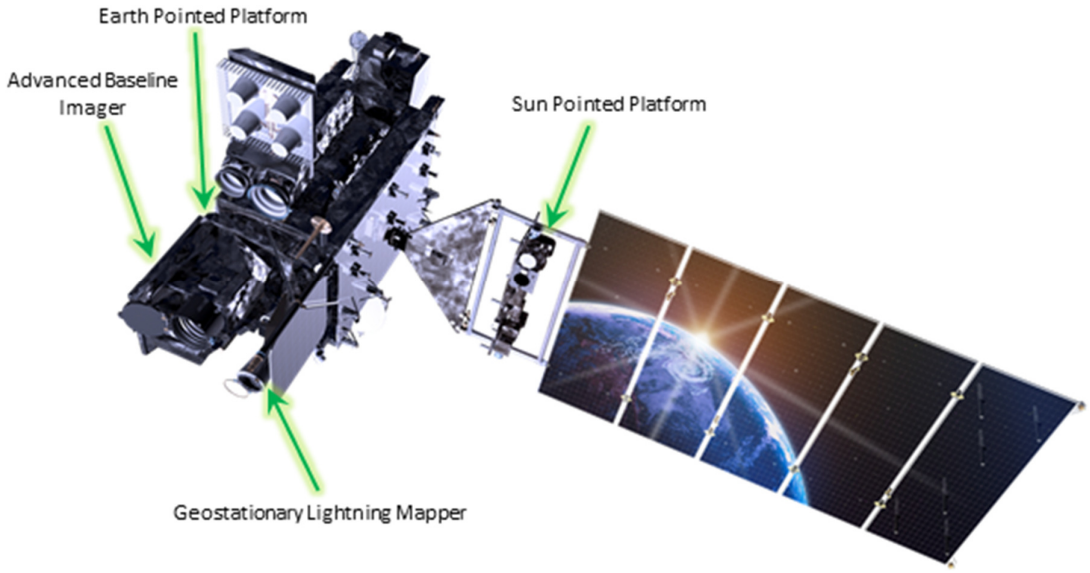

Fig. 1. *GOES-R Spacecraft in Operational Configuration*

In addition to Earth-observing instruments, GOES-R spacecraft also hosts two solar staring instruments on the SPP, a particle detection instrument, and a magnetometer mounted on a deployable boom. The two SPP-mounted instruments have their own highly demanding pointing and pointing stability requirements.

In this paper, we briefly review the performance needed to realize the ambitious GOES-R Image Navigation and Registration (INR) [6][7] objectives. We summarize the performance requirements in the areas of pointing control and low-frequency pointing stability, jitter, attitude and rate knowledge, and orbit knowledge. We then review the key GN&C (Guidance, Navigation & Control) design features implemented on the GOES-R spacecraft to achieve these performance requirements. Finally, we present the flight results for these areas, and examine the effectiveness of the key GN&C design features in achieving the performance requirements. The results show that the GOES-R design is successful in achieving the demanding requirements necessary to accomplish the mission.

2. GOES-R GN&C PERFORMANCE REQUIREMENTS

The increased spatial, spectral and temporal resolution of the GOES-R Earth-observing instruments impose extremely demanding performance requirements on the spacecraft GN&C design, including pointing control, pointing stability, jitter, attitude and rate knowledge, and orbit knowledge. Customer defined GN&C requirements in these areas [5] are summarized in Table 1. The GOES-R pointing and pointing stability requirements are comparable to other precision-pointing missions. However, availability requirements mean the specifications in Table 1 must be met nearly continuously. Meeting these requirements during maneuvers will allow the instruments to continue nominal operations without compromising performance. Maneuvers include operating through daily Momentum Adjustment (MA) events, East-West Station-Keeping (EWSK) and North-South Station-Keeping (NSSK) maneuvers. The next section describes feedforward and calibration techniques to enable these requirements to be met continuously.

Table 1: *Summary of Customer-Defined GN&C Requirements for Earth-Observing Instruments*

Requirement	Value
Attitude Knowledge	
Static	1200 µrad 3σ per axis (prior to on-orbit calibration)
Slow Dynamic	45 µrad 3σ per axis
Dynamic	30 µrad 3σ per axis
Integrated Rate Error	
1 Sec	1 µrad 3σ X/Y axis; 1.5 µrad 3σ Z axis
30 Sec	2 µrad 3σ X/Y axis 2.5 µrad 3σ Z axis
300 Sec	7 µrad 3σ per axis
900 Sec	18.5 µrad 3σ per axis
Latency	Latency requirement curve as discussed in [1][2], <7.5 ms for GOES-R design
Orbit Knowledge	
In-Track Position	75 m 3σ
Cross-Track Position	75 m 3σ
Radial Position	100 m 3σ
Velocity	6 cm/sec 3σ per axis
Pointing Accuracy	207 µrad 3σ per axis
Pointing Stability, 60 sec	224 µrad 3σ per axis
Attitude Rate Error	60 µrad/s 3σ per axis, based upon 7.5 msec latency [1][2]
Jitter	Acceleration and shock response spectra at the instrument interface per Fig. 2
Availability	< 120 minutes per year of lost observation time

Jitter requirements for the nadir pointed instruments have been cast in terms of the linear translational accelerations and shock response spectra (SRS) at the instrument interfaces, as shown in Fig. 2. The spacecraft must achieve its requirement in the presence of the ABI disturbance shown. The "hats" in the acceleration and SRS profiles are allowances for the cryocoolers in the ABI instrument. As can be seen from the plots, this does not leave much room for spacecraft-induced disturbances, such as reaction wheels, thrusters, and gimbal drive mechanisms. The requirements cover a broad frequency range out to 512 Hz, which drives the EPP optical bench to be a stiff design, and drives the EPP to be passively isolated from the spacecraft bus.

The spacecraft is required to provide low-latency 3-axis attitude rate data directly to the ABI instrument at 100 Hz, and is also required to provide inertial attitude knowledge to the instruments at 1 Hz. The ABI instrument uses attitude rate data to provide real-time control of its Line-of-Sight (LOS). The instrument maintains its own internal attitude knowledge to achieve the GOES-R INR performance [8]. For the 100 Hz attitude rate data provided to ABI, the GOES-R spacecraft has a unique set of specifications. Rather than specifying the rate errors in terms of traditional Farrenkopf gyro model parameters [9] (angle white noise, angle random walk, and rate random walk) GOES-R defines performance in terms of Integrated Rate Error (IRE), which specifies 3-axis integrated rate accuracy over various time intervals. As an attitude knowledge requirement, IRE is distinct from a pointing stability requirement, which represents a limit on the physical motion of the

spacecraft over some specific time interval. Instead, IRE represents a knowledge error over a specific time interval, regardless of physical motion.

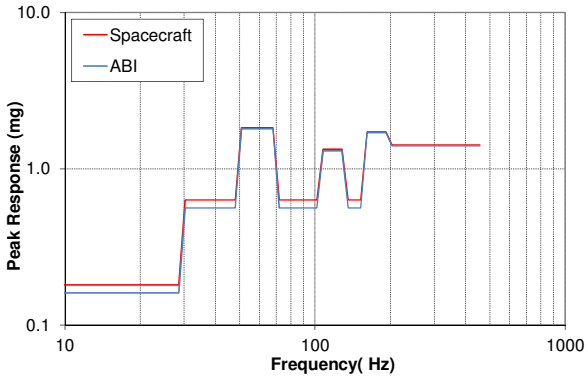

Fig. 2a. Linear translation acceleration limits on the EPP.

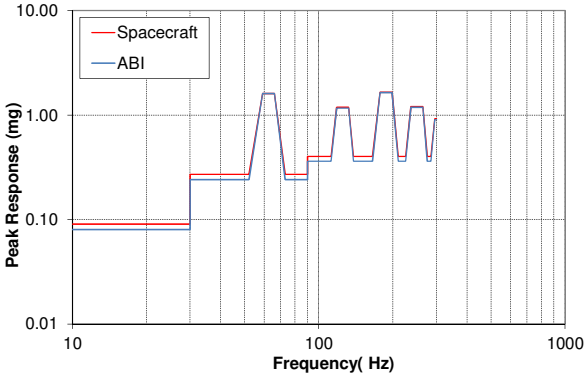

Fig. 2b. Shock response spectra limits on the EPP.

The GOES-R GN&C is also required to provide accurate orbit position and velocity to the instruments at 1 Hz. Traditional methods of providing orbit knowledge would be cumbersome and labor-intensive given the tight requirements shown in Table 1. Instead, GOES-R incorporates an on-board Global Positioning System Receiver (GPSR) to provide orbit data with the specified accuracy. Because GOES-R is a GEO satellite, this involves tracking extremely low level signals while operating above the GPS constellation [10][11][12][13].

3. GOES-R GN&C DESIGN APPROACH

The stringent GOES-R attitude determination requirements dictate that the IMUs and star trackers be co-located with the Earth-observing instruments on the EPP. To meet the jitter requirements presented in the previous section, the EPP is designed as a stiff structure with the first structural mode at approximately 50 Hz. The EPP is constructed of carbon fiber facesheets over aluminum honeycomb, spans approximately 1.9 x 2.2 m, and has a thickness of about 0.15 m. The resulting configuration is shown in Fig. 3, where the placement was driven by fields of regard for the instruments, and keep-out zones for the star trackers. The high stiffness of the optical bench readily transmits disturbances through the structure. To attenuate high frequency disturbances to the Earth-observing instruments, including reaction wheel disturbances, gimbal disturbances, and disturbances from the sun-pointed instruments, the EPP is passively isolated from the spacecraft bus with Honeywell D-Strut isolators [14] arranged in a modified Stewart-platform configuration [15][16]. The isolation system provides attenuation for frequencies above ~5 Hz in all six degrees-of-freedom.

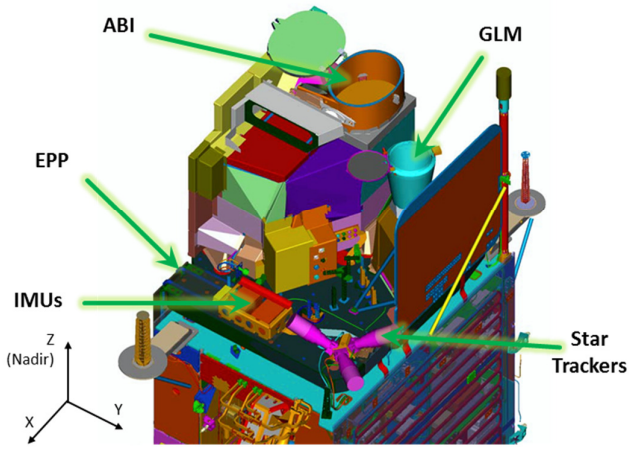

Fig. 3a. Earth Pointed Platform Configuration for GOES-R

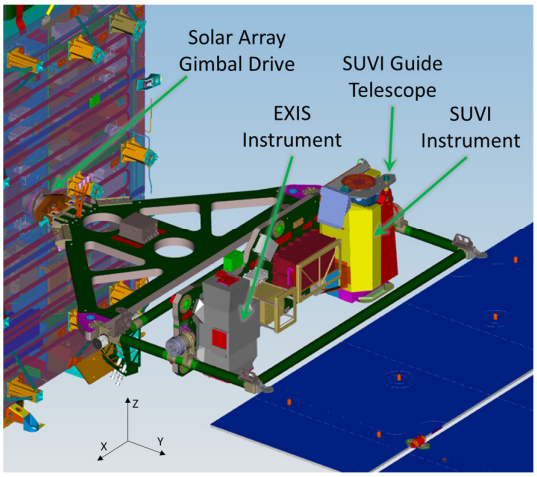

Fig. 3b. Sun Pointed Platform Configuration for GOES-R

The GOES-R spacecraft design utilizes 6 Honeywell HR-18 reaction wheels, arranged as shown in Fig. 4. The wheels are mounted at the –Z end of the vehicle, far away from the EPP to reduce vibration to the instruments. The use of 6 wheels provides functional redundancy, reduced maximum speed (which decreases vibration), and relatively high torque capability. A secondary passive isolation system manufactured by Moog/CSA Engineering is implemented for each reaction wheel. The design is based upon Moog's Visco-Elastic Material (VEM) vibration isolation technology [17]. This secondary isolation system provides attenuation for frequencies above ~50 Hz for each wheel.

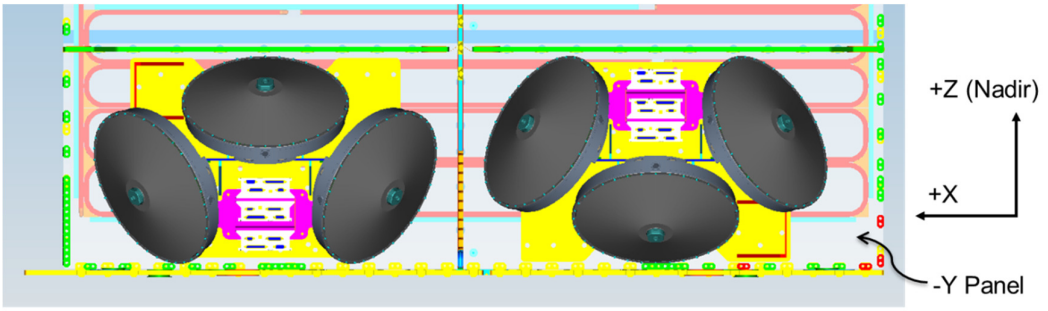

Fig. 4. *Reaction Wheel Configuration of the GOES-R Spacecraft*

The "operate-through" capability is unique to the GOES-R mission, and drove the need to develop Aerojet Rocketdyne's 0.09 N Low Thrust REA (LTR) for use during Momentum Adjust (MA) events and EWSK maneuvers. The 0.2 N arcjet thrusters (also built by Aerojet Rocketdyne) are used for NSSK because of their high Isp of ~570 sec. The torque from both of these thruster types can be balanced by the reaction wheels.

Within the control design, there are a number of feedforward paths to facilitate the operate-through capability. Feedforward of the thruster torques during thruster operations is one feedforward path. Additionally, ABI provides force and torque disturbance predictions for scan mirror motion. Freesland et al. [18], demonstrated the effectiveness of using Predicted Interface Force and Torque (PIFT) data to improve attitude stability performance by a factor of 5X. GOES-R includes feedforward compensation based on ABI's PIFT data.

To reduce the impact of low frequency disturbances, GOES-R has included Active Vibration Damping (AVD) developed by Lockheed Martin [19][20]. This additional compensation phase stabilizes the first several structural modes, up to ~2 Hz. The first structural mode is at ~0.25 Hz, and is related to the large solar panel flexibility coupled with the deployment hinge stiffness. Although not truly a feed forward term, the AVD compensation is implemented within the architecture in a similar fashion. It has proven particularly effective for the first three structural modes on GOES-16.

Finally, the gimbal design used for the azimuth and elevation control of the solar array and SPP incorporates the proven low-disturbance design first implemented on the Mars Reconnaissance Orbiter [21]. The design is based upon a zero-backlash harmonic drive with a relatively high gear reduction of 200:1. A 2-phase brushless motor with sine-drive commutation provides a low disturbance capability, and effectively eliminates motor cogging. A high-bandwidth motor-rate control loop eliminates most of the harmonic drive friction and nonlinear effects. The high performance of the gimbals removes gimbal dynamics as a significant pointing and jitter disturbance source, while providing sub-arcsec pointing capability.

4. POINTING CONTROL AND LOW-FREQUENCY POINTING STABILITY

There are common disturbances for all operational scenarios which affect low frequency pointing performance. These include solar array articulation, ABI scan mirror disturbances, and reaction wheel friction, gyroscopic, and zero-speed crossing disturbances. In addition to these continuous disturbances, periodic MA events and EWSK/NSSK maneuvers produce uncompensated thrust and torque variation. Although GOES-R Flight Software (FSW) uses feedforward to improve pointing stability, calibration residuals and statistical variation

limit the performance. In this section, we discuss the effectiveness of several key design features of the GOES-R control implementation, including thruster calibration and feedforward for MA events and NSSK/EWSK maneuvers, PIFT compensation for instrument scanning disturbances, and AVD mitigation of flexible body modes. We then present the results of implementing Markley's redundancy management algorithm for reaction wheels [22], which is used to manage the null-space momentum of vehicle's six reaction wheels. Finally, we highlight the SPP control performance, which uses the Solar Ultraviolet Imager (SUVI) instrument's Guide Telescope (GT) to orient the spacecraft gimbals which provide the precision instrument pointing.

4.1 Thruster Torque Feedforward Approach and Calibrations

As discussed earlier, the GOES-R spacecraft is required to meet all instrument pointing requirements with less than 120 minutes per year of lost observation time. This means that the spacecraft must meet payload pointing requirements during MA events and NSSK/EWSK maneuvers. MA maneuvers are conducted using 0.09 N Aerojet Rocketdyne Low Thrust REAs (LTRs). Orbit longitude control is also accomplished using LTRs for EWSK burns. NSSK inclination control maneuvers burns are conducted every four days using 0.22N arcjet thrusters, also manufactured by Aerojet Rocketdyne. During MA, EWSK, and NSSK maneuvers spacecraft attitude control is maintained using the six reaction wheels.

LTRs are an enabling technology for GOES-16 and were developed for GOES-R over a period of 4 years. LTRs have a steady-state thrust level of 0.09 N at a propellant feed pressure of 270 psi, and have an Isp of greater than 170 seconds for firings 60 seconds and longer. They exhibit a slow and predictable thrust rise, which FSW estimates onboard for each LTR during MA and EWSK maneuvers. The FSW uses predicted LTR thrust profiles in conjunction with ground-measured thruster geometries and the estimated spacecraft Center of Mass (CM) location to calculate feedforward torques for the six reaction wheels. As shown in Fig. 5, the spacecraft has 16 LTRs: 8 on the north panel, 4 on the east panel, and 4 on the west panel. Arcjets have slightly larger thrust than LTR's, with a steady-state thrust level of 0.22 N at a propellant feed pressure of 270 psi. Arcjets have an Isp of greater than 570 seconds for firings 240 seconds in duration and longer. Like the LTRs, they exhibit slow and predictable thrust rise that allows the torque they impart to be predicted and fed forward.

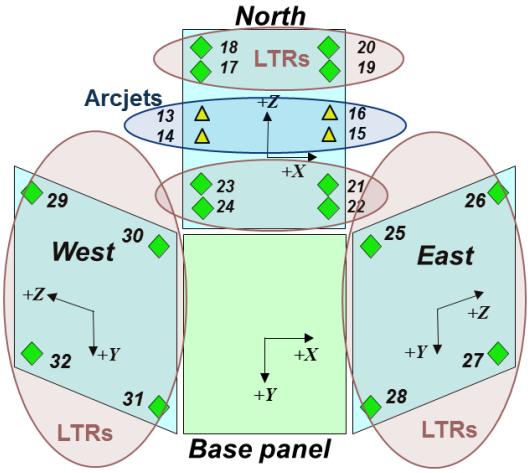

Fig. 5. *GOES-16 Arcjet and LTR Thruster Locations*

To meet the operate-through requirements, onboard estimates of the thruster torque profiles are used to command counteracting reaction wheels torques. Uncertainties in alignments, thruster performance, and plume impingement effects mandate that the compensation parameters be determined in flight through calibration maneuvers. The LTR and arcjet thruster calibration data are processed on the ground to adjust onboard FSW parameters used to calculate feed forward torques. During each calibration maneuver, the vehicle is held in a nadir pointed attitude under reaction wheel (RW) control. With only small environmental torque accumulation during the calibration period, the momentum history allows direct measurement of the torque imparted from each thruster firing. The momentum can be differentiated to compute inertial torque, which is converted to the

body frame using the spacecraft attitude estimate. A priori knowledge of thruster geometry and spacecraft center of mass are combined with observed spacecraft torque to derive thrust profiles for each thruster. During calibration maneuvers, the LTRs are fired individually while high rate telemetry is collected. Updated parameters for MA and EWSK maneuvers are derived from the 20 Hz momentum data collected.

The arcjet thruster calibrations are more complex because arcjets can operate both unaugmented (no arc), and augmented (with an arc). Additionally, multiple power levels are available for augmented operation. Telemetry data collected during three separate calibration events are used to generate thrust profiles for each of the four arcjets. During the first calibration event, each arcjet is fired individually in the unaugmented mode. During two subsequent arcjet calibration events, pairs of arcjets are fired in the augmented mode, and slowly stepped through each of four arcjet power levels. Telemetry data are collected at 20 Hz during each of these events. From these three arcjet calibration events, five thrust profile tables are derived. The first table contains the unaugmented thrust vs. time for each of the four arcjets, while the remaining four tables contain thrust vs. time profiles for each of four augmented power levels.

Fig. 6a shows representative results from the LTR calibration. The two traces shown in the plot represent thrust rise over time for LTR17: the first is the torque from telemetry and estimated torque from the thruster calibration, and the second is the torque error the FSW parameters calculated as a result of the calibration. Likewise, Fig. 6b shows the equivalent results from the arcjet calibration.

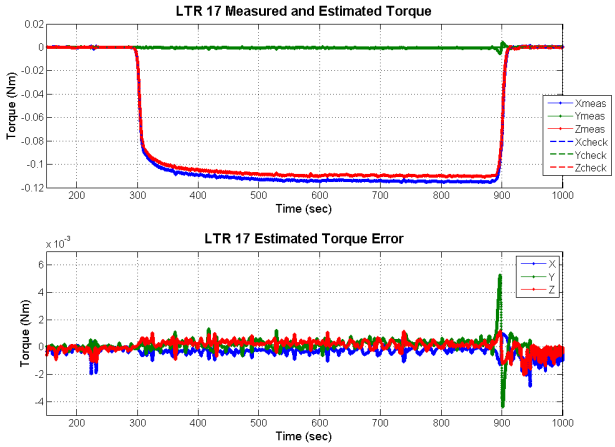

Fig. 6a. *Representative LTR Calibration Results*

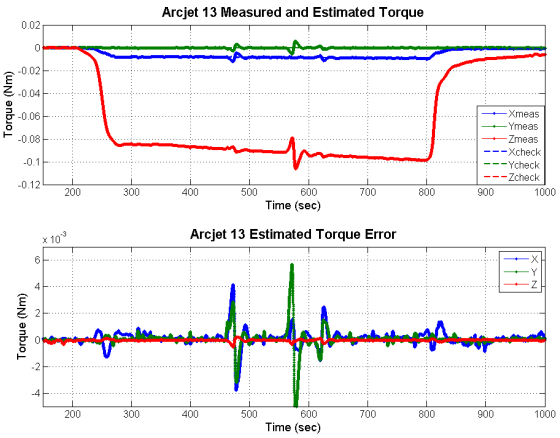

Fig. 6b. *Representative Arcjet Calibration Results.*

The LTR and arcjet feed forward parameter derivations assume accurate knowledge of thruster locations, nozzle directions, and spacecraft CM. These are used to compute LTR and arcjet thrust profiles from the high rate spacecraft telemetry. Once thrust profiles of individual thrusters are derived, cross-check computations can be performed using $\tau = r \times F$, where τ is torque, r is the moment arm from the thruster to the spacecraft CM, and F is the thruster force level. For the unaugmented arcjet calibration, x-axis torque errors of approximately 3 mNm were consistently noted for all four arcjets when running this cross check. The cross-check was repeated for the LTR calibrations, and torque errors of similar magnitude were observed. This discrepancy indicated an erroneous CM estimate of roughly 4 cm. The CM was adjusted to reduce the torque prediction errors, which produced torque errors of less than 1 mNm for all arcjets and LTRs except for LTR 32. The results presented in Fig. 6a and Fig. 6b include the CM correction, and show excellent agreement between the modeling and the flight telemetry. The ~5 mNm transient errors observed in both Fig. 6a and Fig. 6b have been correlated to reaction wheel zero speed crossings. These transients are brief, and do not affect the overall accuracy of the calibrations.

Additional investigation into the mismatch of LTR 32 relative to the other LTRs showed some plume impingement effects for LTR 32. Plume effects can be readily accommodated by adjusting the thruster location

and alignment parameters. The analysis produced small adjustments for the LTR 32 position and orientation, which were updated along with the revised CM location and new arcjet and LTR feed forward parameters.

On-orbit data were collected for NSSK, EWSK, and MA maneuvers before and after FSW parameter updates based on the calibrations. The results are shown in Fig. 7, and summarized in Table 2. As seen in the plots, the active LTR and arcjet calibrations provide reduced attitude errors during the maneuvers. The errors were within the 207 µrad sub-allocation prior to the calibrations for MA and EWSK. This indicates reasonably accurate ground CM and alignment measurements, as well as accurate feedforward parameters pre-launch. However, the NSSK produced out-of-specification disturbances prior to calibration. The post-calibration results are compliant with the 207 µrad requirement. Because of FSW implementation details, feedforward generally provides better transient mitigation at the start of maneuvers than at the end of maneuvers.

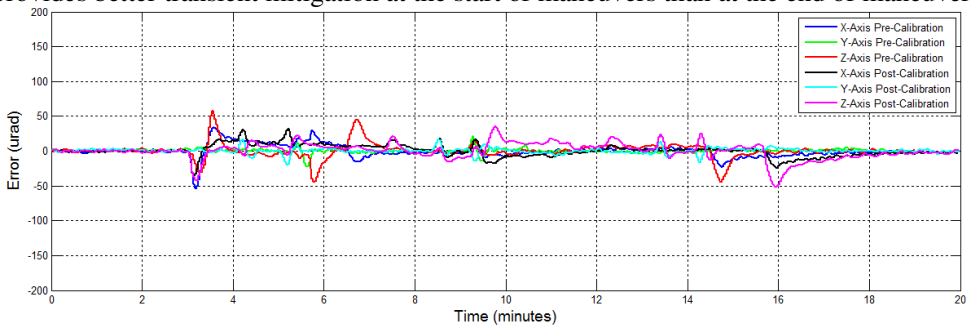

Fig. 7a. *MA Attitude and Rate Errors Before and After LTR Calibration.*

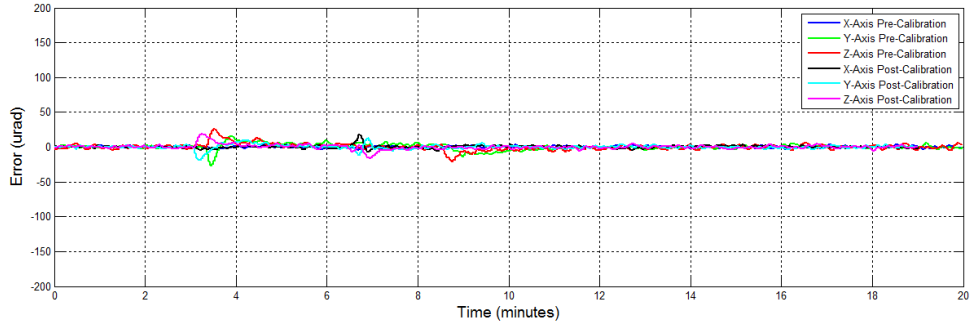

Fig. 7b. *EWSK Attitude and Rate Errors Before and After LTR Calibration.*

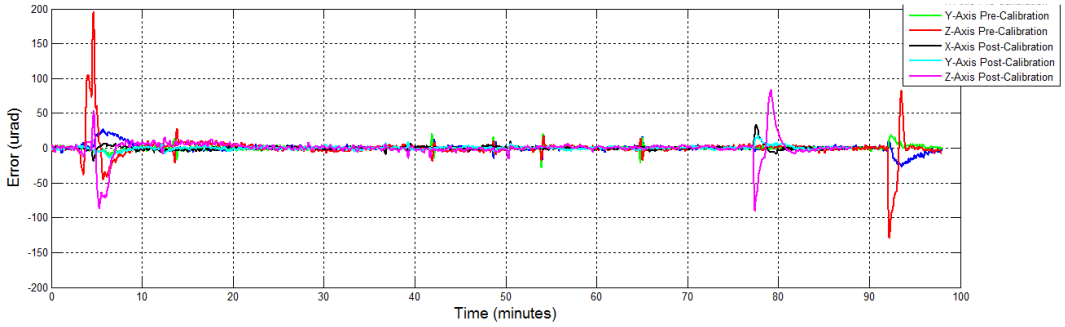

Fig. 7c. *NSSK Attitude and Rate Errors Before and After Arcjet Calibration.*

Table 2: *Summary of GOES-16 Attitude Control Performance for Various Maneuvers*

Requirement	Momentum Adjust		EW Stationkeeping		NS Stationkeeping	
	Pre	Post	Pre	Post	Pre	Post
Attitude Error, <207 µrad 3-σ/axis	57	52	27	19	196	90
Attitude Stability, 60 sec, <224 µrad 3-σ	88	61	42	29	238	141
Attitude Rate Error, <60 µrad/s 3-σ	13	7	6	4	20	15

4.2 Predicted Interface Forces and Torques (PIFT) Compensation

The ABI instrument has two disturbance sources for which the instrument provides time-tagged PIFT data. First, the instrument has two internal scan mirrors, North-South (NS) and East-West (EW), which provide torques about the instrument X- and Z-axes, respectively. The scan mirrors are active while ABI is powered and operational. Second, the instrument has a solar calibration cover which provides forces along the instrument X- and Y-axes and torque about the instrument Z-axis. The solar calibration cover is operated relatively infrequently (monthly), so will not be discussed in detail here. ABI provides PIFT data packets at 20Hz containing predicted forces and torques, along with predicted timing.

PIFT is fed forward into the attitude controller to compensate for ABI disturbances. Predicted forces are converted to torques using configurable moment arm, and summed with predicted torques. PIFT data are multiplied by a configurable gains to correct polarity, and to allow corrections for any performance discrepencies in flight. The FSW issues reaction wheel torques at the time embedded with the PIFT data packet, with additional timing correction for known delays within the system. During the design effort for GOES-R, a 70 millisecond timing error between actual ABI disturbances and a control system response was assumed. This consisted to a 50 ms error (one frame) in system response, and a 20 ms PIFT timing error between PIFT predicted time and the realization of ABI disturbances. The accuracy of the ABI PIFT time tag and the reaction wheel torque command timing was verified prior to launch. But, ground verification of PIFT polarity proved to be extremely difficult, so there were no definitive ground tests to prove the implementation was correct.

For GOES-16, example motion of the ABI instrument's scan mirrors is shown in Fig. 8a. The motion is typical of normal observations of the continental United States (CONUS). The effectiveness of the PIFT compensation is shown in Fig. 8b. The timeframe shown is the same 35 minutes as presented in Fig. 8a, where the ABI instrument is scanning continuously. The PIFT feed forward compensation is enabled at approximately 14 minutes, as denoted by the red vertical line. Prior to the PIFT compensation being implemented, the rate disturbances from the scan mirrors are approximately 10 μrad/s in the Z-axis. After the compensation is enabled, the response is reduced by an order of magnitude. Significantly smaller responses are also apparent in the X- and Y-axes. This represents exceptional performance considering that the reaction wheels are mounted on the opposite end of the spacecraft from the ABI instrument.

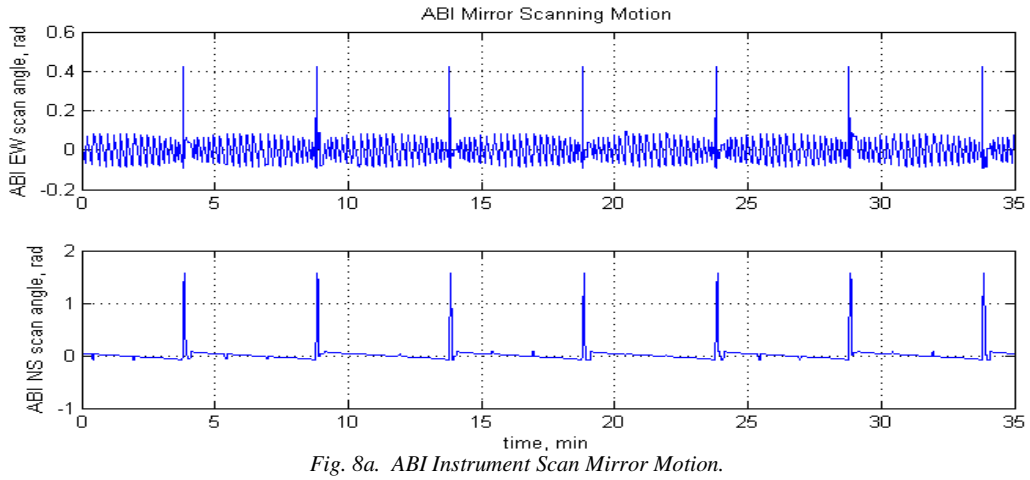

Fig. 8a. ABI Instrument Scan Mirror Motion.

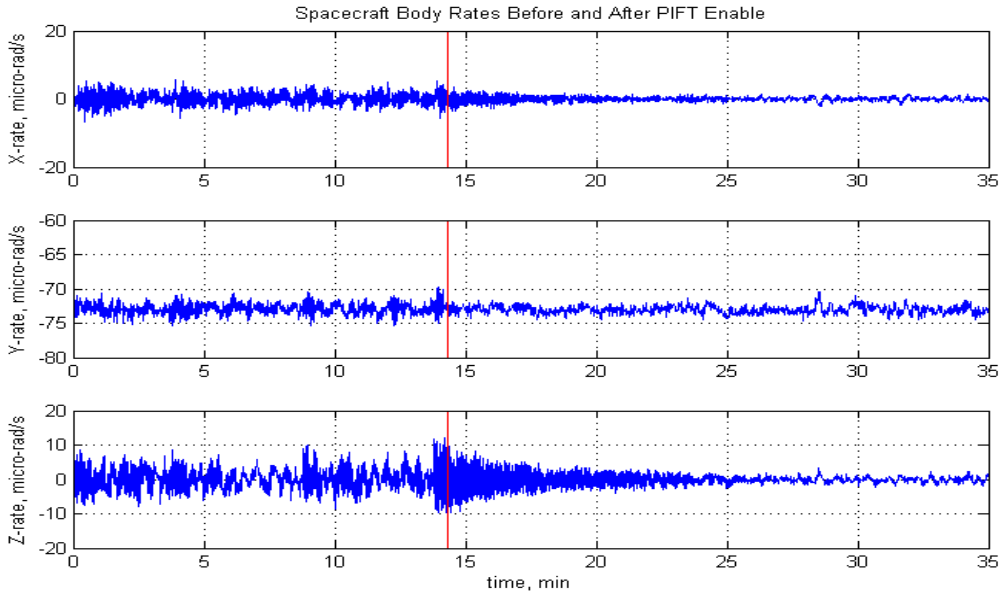

Fig. 8b. *Spacecraft Body Rates during ABI Scanning, before and after Enabling PIFT Compensation.*

4.3 Active Vibration Damping Compensation

The GOES-R vehicles have several flexible appendages with multiple modal frequencies below 3 Hz, which can result in undesirable pointing perturbations. In order to meet GOES-R pointing and pointing stability requirements, GOES-R implements AVD compensation operating in parallel with the nadir pointing attitude control. Details of the implementation and GOES-16 flight results are presented in [19], and are only summarized here. AVD commands reaction wheels torques based upon 20 Hz gyro data, providing additional damping for modes below 3 Hz. The flexible modes vary with the solar array angle, so a modal mapping is needed for 360 degrees of solar array gimbal motion. The AVD compensation uses this mapping to provide appropriate modal compensation based upon solar array gimbal angle and sensed body rates. AVD applies phase stabilized compensation at the appendage mode natural frequencies. This increases modal damping and attenuates appendage vibration, thereby improving pointing performance. Additionally, AVD increases low-frequency disturbance rejection. GOES-R implements AVD as single-input, single-output rate compensation for each body axis.

As shown in Fig. 9, AVD consists of three components: a FSW algorithm performing on-orbit modal excitation, a ground-based system identification process, and a FSW algorithm implementing AVD compensation. The full torque capability of the reaction wheels is used to provide dynamic excitation of the flexible body modes. The modal excitation consists of 20 Hz pseudo-random reaction wheel torque commands over a single orbit. Time-correlated angular rate data is collected at 20 Hz over this period. Ground processing of flight telemetry produces a Fourier model parameterized by solar array gimbal angle. Additional analysis selects the AVD compensation, providing both acceptable tracking performance and modal attenuation. The identified Fourier model coefficients and the AVD controller gains are then uplinked to the spacecraft. Only after calibration and gain selection are valid AVD parameters available onboard—the AVD parameters are all zero at launch. The AVD compensation FSW selects the appropriate coefficients based upon solar array gimbal angle, applies those coefficients to the angular rate data, and outputs reaction wheel torque commands.

Fig. 9. *AVD Implementation Approach*

For GOES-16 with a solar array gimbal angle of 105 deg, Fig. 10 shows the yaw-axis transfer function from disturbance torque input to angular rate output for both AVD compensation enabled and disabled. The modal damping increase provided by AVD can clearly be seen. The AVD compensation increases modal damping significantly for three appendage modes at this gimbal angle, as summarized in Table 2. In particular, AVD provides ~7X increase in the damping of the solar wing out-of-plane fundamental bending mode.

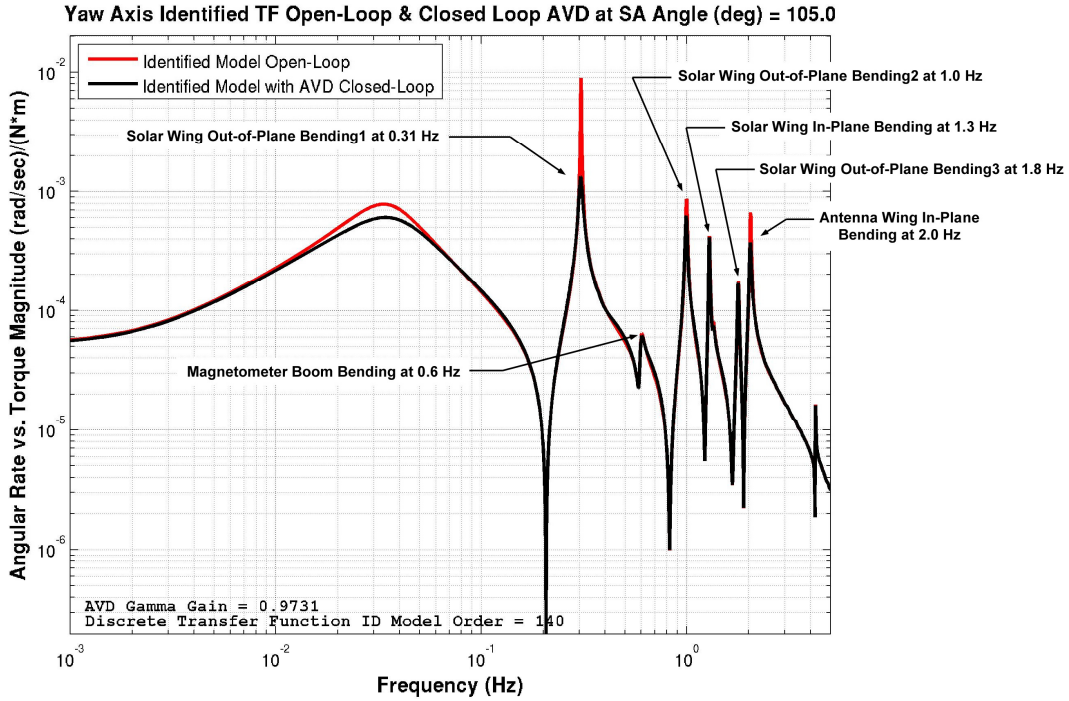

Fig. 10. *GOES-16 Disturbance Rejection Transfer Function with AVD Disabled and Enabled*

Table 3: *Modal Damping Increase Provided by the GOES-16 AVD Controller*

Mode Description Yaw Axis at 105° SADA Angle	Frequency (Hz)	Damping Ratio (%) Identified	Damping Ratio (%) with AVD	AVD Damping Factor
Solar Wing Out-of-Plane Bending I	0.31	0.257	1.815	7.1
Solar Wing Out-of-Plane Bending II	1.00	0.626	0.879	1.4
Antenna Wing In-Plane Bending	2.04	0.480	0.845	1.8

Note: AVD Damping Factor = (Modal Damping w/AVD)/(Modal Damping w/o AVD)

The performance impacts are most evident at the beginning and end of the various thruster operations, namely MA, NSSK, and EWSK. An example of the performance improvement with AVD is shown in Fig. 11. At the end of NSSK maneuvers, a small attitude transient is typically observed. The thruster torque transient and the control activity to remove the transient can excite the low frequency appendage modes. The end of the NSSK occurs at the 3 min mark in Figure 11, and the transient response can easily be seen. Regardless of whether AVD is enabled or disabled, the attitude transient and recovery are complete within 2 min. But prior to enabling AVD, appendage oscillations of up to 10 µrad/s are observed in the X-axis, and they persist for more than 15 min. The transient is slightly smaller when AVD is enabled, but the 10 µrad/s oscillations are no longer present at all. AVD is very effective in damping the appendage mode. More details on the AVD implementation and performance are presented in [19].

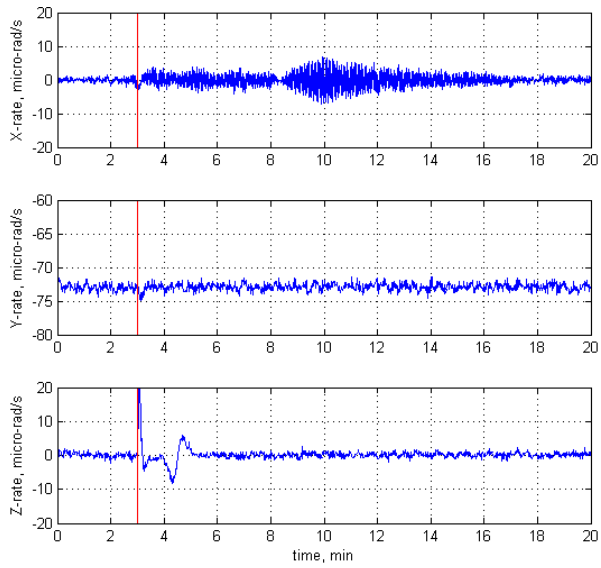

Fig. 11a. Rate Transients at end of NSSK, AVD Disabled

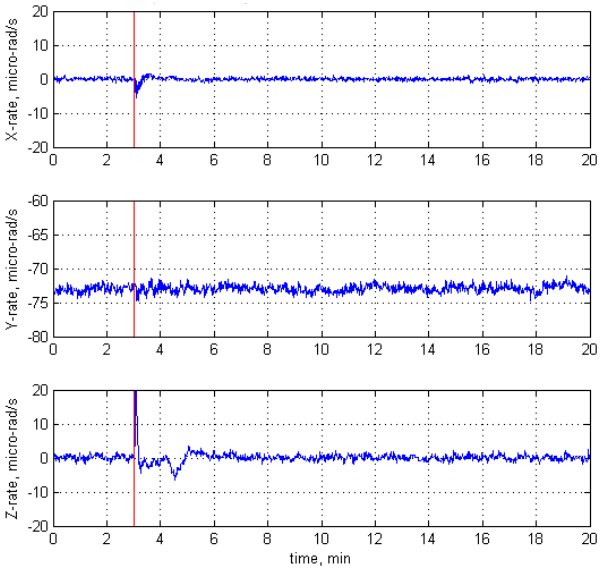

Fig. 11b. Rate Transients at end of NSSK, AVD Enabled.

4.4 GOES-R Reaction Wheel Redundancy Management

As shown in Fig. 4, GOES-R uses six reaction wheels to apply control torques to the three spacecraft. The geometry of the RW configuration is shown in Fig. 12. The null space of the RW suite is 3-dimensional, and thus there are an infinite number of RW momenta combinations that result in the same spacecraft momentum state. For GOES-R, the algorithm used to convert a 3-axis body frame momentum command into six RW momentum commands is based on [22], which minimizes the infinity norm of RW momentum commands. In this paper, we refer to this as the "Markley algorithm," after the principal author.

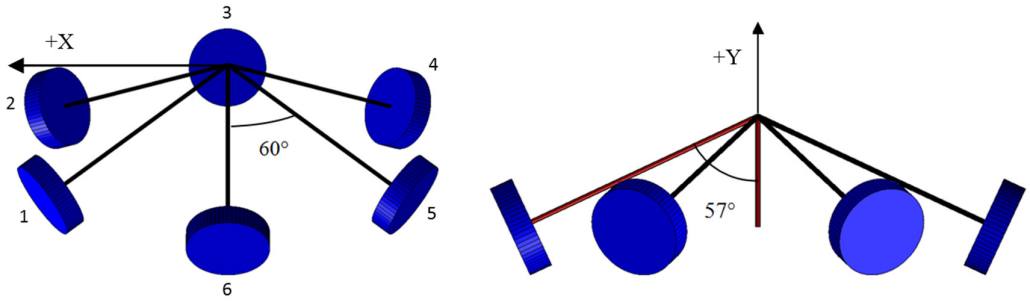

Fig. 12. Geometric Representation of the GOES-16 Reaction Wheel Configuration

For the GOES-R configuration, application of the Markley algorithm to body frame torque commands results in four or more reaction wheels receiving a torque command with the same magnitude. The magnitude of the torque commands sent to the remaining reaction wheels is less than or equal to the magnitude sent to the first four. This technique allows the 6-RW suite to produce up to 33% more body frame torque than provided by the more common pseudo-inverse solution to command redundant reaction wheels. The algorithm described in [22] is also used to calculate the minimum infinity norm momentum state of the six reaction wheels. The minimum infinity norm momentum solution minimizes the maximum RW speed, which allows the 6-RW suite to store up to 33% more body frame momentum than provided by the more common pseudo-inverse approach.

Normal torque commanding of the reaction wheels results in the reaction wheel momentum state diverging from the minimum infinity norm momentum solution over time. Consequently, a secondary reaction wheel null torque controller is required to keep the momentum state of the reaction wheels close to the minimum infinity norm solution. RW torques commanded by this controller are in the RW torque null space and do not

result in body frame torques. Consequently, this is called the RW null torque controller. A simplified block diagram of the null torque controller implementation is shown in Fig. 13. Note that torque commands are limited to ensure that the null torque controller does not interfere with the primary attitude control law, which could cause a loss of attitude control authority and a corresponding degradation in pointing performance.

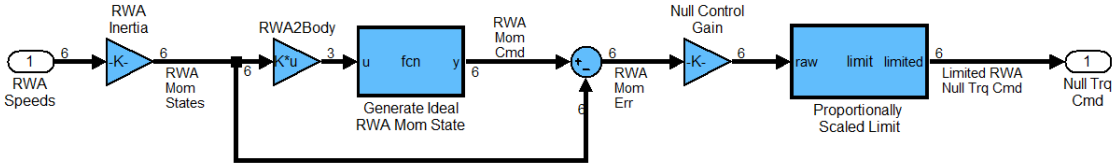

***Fig. 13**. Reaction Wheel Null Torque Controller Block Diagram.*

Fig. 14 plot shows predicted and actual reaction wheel momentum states for GOES-16 during a typical day. The rapid change in RW momentum is due to the daily momentum adjust, which is required to account for the up to ~80 Nms of momentum per day the spacecraft accumulates due to solar radiation torque. As seen in Fig. 14, the Markley algorithm works well in managing momentum for the redundant wheel configuration, and the on-orbit results closely match simulation predictions.

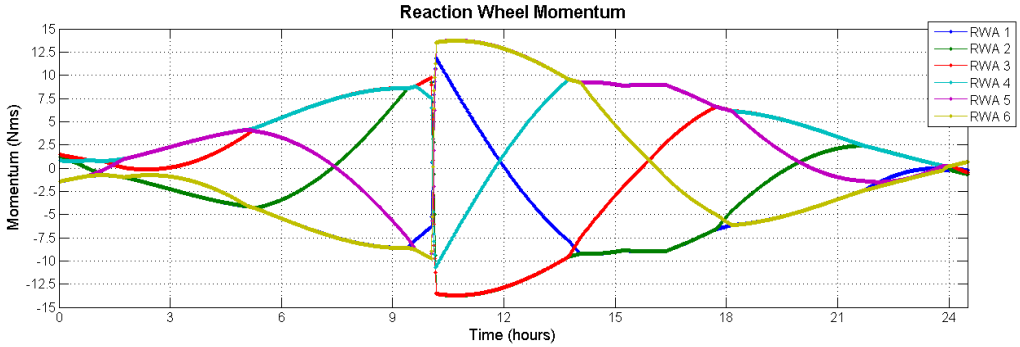

***Fig. 14a.** Simulated Operations Reaction Wheel Momentum*

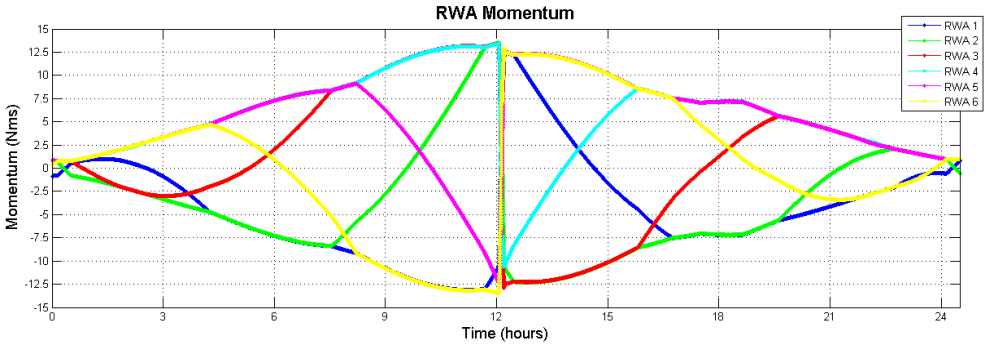

***Fig. 14b.** On Orbit Measured Reaction Wheel Momentum*

4.5 SPP Pointing and Pointing Stability

The SPP instrument configuration for GOES-R is unique in that the arcsec-level sun-pointing accuracy is provided by the spacecraft gimbal control based upon data provided by the SUVI instrument. The SUVI and the Extreme Ultraviolet and X-ray Irradiance Sensors (EXIS) instruments are co-aligned on the SPP prior to launch. Centering the sun within SUVI GT's field of view provides the required instrument pointing for both EXIS and SUVI. The spacecraft gimbal control first uses attitude knowledge and sun ephemeris information to command the gimbal angles such that the sun is within the SUVI GT's 48 arcmin field of view. The FSW then autonomously switches to closed-loop control using data received from the GT. The GT has extremely good performance, with resolution of better than 0.25 arcsec and noise equivalent angle (NEA) of less than 0.4 arcsec. This performance supports nominal SPP pointing errors of less than 1 arcsec. Filtered spacecraft

body rates are also fed into the gimbal control law and used to take out spacecraft body motion. This enables the low bandwidth gimbal control law to meet the tight pointing stability requirements for the SPP instruments, even during periodic thruster events such as MA, EWSK, and NSSK.

The driving requirement for SPP instrument pointing is the requirement to provide radial pointing stability over 60 seconds of better than 5.5 arcsec, 3-σ. Pre-launch analysis and simulation, including a worst-case stack up of disturbances and misalignments, indicated that the NSSK maneuvers would be the most challenging scenario for meeting this requirement. Throughout development, typical performance for the radial pointing stability requirement during MA and EWSK maneuvers was less than 2 arcsec. Because of the predicted and observed margins for those cases, only the more stressing NSSK case is presented here.

GOES-16 SPP pointing during MA, EWSK, and NSSK maneuvers have been analyzed for compliance against the requirements. Data from before and after the thruster calibrations discussed above have been assessed. Development efforts showed the radial pointing stability requirement to be especially challenging to meet because of various nonlinearities in the gimbals themselves. All flight data show that the SPP pointing performance is within analytical predictions, with post-calibration cases showing improved performance versus pre-calibration cases. The results are summarized in Table 4. As expected, SPP radial pointing stability performance during MA and EWSK maneuvers easily meets requirements, with errors less than 2 arcsec. SPP radial pointing stability performance during NSSK maneuvers also meets requirements, with post-calibration slightly better than predictions. The results for a typical NSSK maneuver are shown in Fig. 15. As with the EPP pointing performance, the largest errors occur during the NSSK startup and shutdown attitude transients.

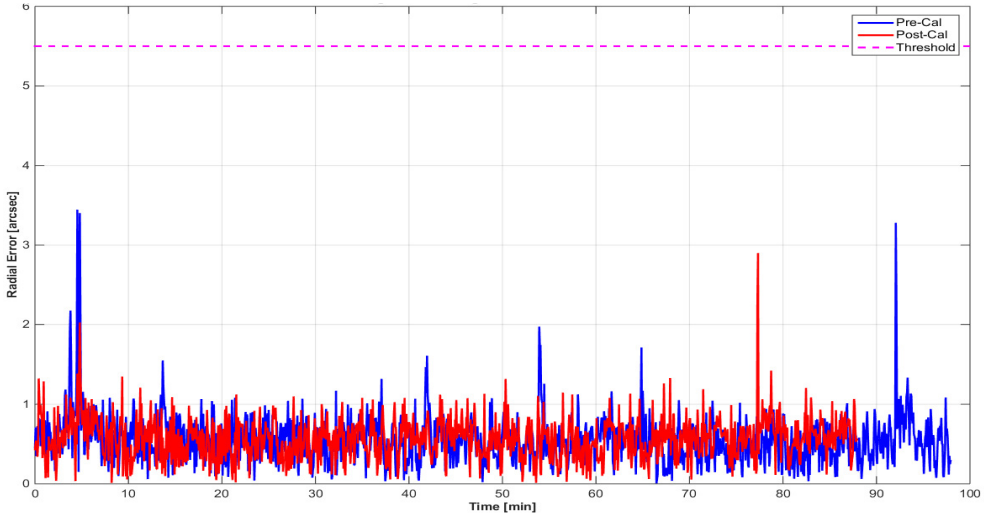

Fig. 15. *SPP Radial Pointing Error during Pre-Cal and Post-Cal NSSK Maneuvers*

Table 4: *Summary of GOES-16 SPP Control Performance for Various Maneuvers*

Requirement	Peak (arcseconds)			
	Nominal	MA	EWSK	NSSK
Radial Pointing Stability, 60 sec, <5.5 arcsec 3-σ	1.17	1.87	1.45	2.9

The results shown above demonstrate the excellent pointing performance achieved for the SPP instruments. The results were only made possible by the high performance gimbal design, including the high bandwidth inner rate loop to mitigate the nonlinearities inherent with the harmonic drive mechanism. The gimbal implementation along with good calibration results facilitate arcsec-level pointing performance using spacecraft appendage articulation.

5. DUAL-ISOLATION AND JITTER PERFORMANCE

Along with the instrument suite's improved resolution and performance came increased sensitivity to disturbances over a broad spectrum. For GOES-R, the sensitive frequency range is 0-512 Hz. As discussed earlier, EPP isolation attenuates bus disturbances to the Earth-observing instruments, implementing Honeywell D-Strut isolators between the spacecraft bus and the EPP. The GOES-16 implementation is shown in Fig. 16. The EPP isolation provides disturbance attenuation above ~5 Hz. The attenuation performance was verified prior to launch in the configuration shown. Originally this configuration was considered sufficient to provide isolation from all spacecraft bus disturbances, including the reaction wheels. However, uncertainties associated with a late change in reaction wheel suppliers, along with analysis showing a potential sensitivity to resonances in the new reaction wheel housing, led the program to add additional isolation at the reaction wheel mounting interfaces. The reaction wheel isolation attenuates disturbances above ~50 Hz, which addresses the high-frequency reaction wheel housing resonances. Details of the EPP and reaction wheel isolation, including qualification and performance verification activities, are provided in [15].

Fig. 16. *EPP flight configuration of GOES-R (prior to final thermal blanket installation)*

The EPP provides a stable platform for the two Earth-observing instruments, ABI and GLM, and the attitude determination sensors, IMUs and star trackers. The implementation provides quasi-kinematic mechanical mounting of the instruments, power and data interfaces, grounding, and thermal interfaces. Alignment stability requirements are extremely tight: changes due to thermal distortion are budgeted to be less than 50 µrad over an orbit. Due to the large combined EPP and instrument mass of ~530 kg, launch locks are employed to carry the launch loads, which restrain the EPP during launch. Typically launch locks are released immediately after achieving the desired orbit. On GOES-16, however, release was delayed by several months to allow collection of ABI and GLM science data before and after launch lock release. This approach, along with the availability of 6 seismic EDAs (EPP Diagnostic Accelerometers) sampled at ~2 KHz and with IMU gyro data sampled at 200 Hz, afforded a unique opportunity to assess the effectiveness of isolation. Fig. 17 shows representative responses before and after releasing the launch locks on GOES-16. All science instruments were operating in their nominal data collection modes, which can be seen by the peaks in the response caused by ABI's cryocoolers. The responses shown include both MA events and NSSK maneuvers, while the SPP was tracking the sun with both gimbals. This scenario represents a stressing scenario for the spacecraft disturbance envrionment to the EPP. As can be seen in Fig. 17, both the undeployed and the deployed EPP configuration meet the overall disturbance requirements. Because ABI's cryocoolers are internal to the instrument located on the EPP, the EPP isolation cannot provide attenuation for those disturbances. Significant attenuation is observed in the background environment in between the cryocooler peaks. Further detail on the EPP and reaction wheel isolation on-orbit performance is presented in [16].

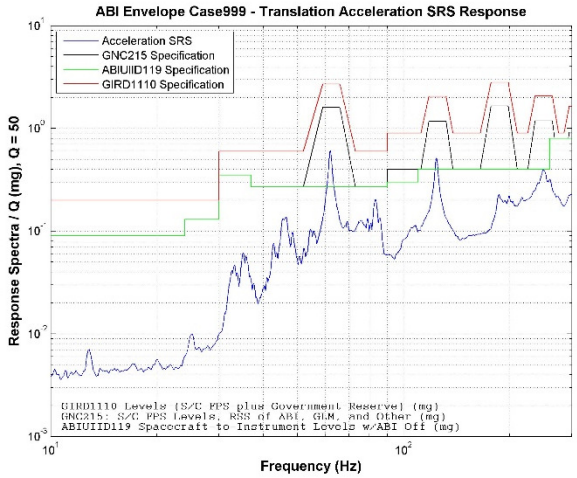

Fig. 17a. *GOES-16 Shock Response Spectrum Pre-EPP deployment (RWA isolation only)*

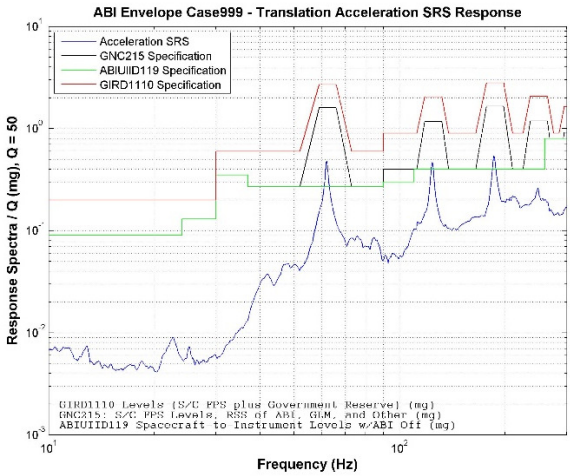

Fig. 17b. *GOES-16 Shock Response Spectrum Post-EPP deployment (Dual isolation)*

Based upon the responses shown above and additional results presented in [16], it is clear that the GOES-R design meets the bus disturbance attenuation requirements with margin. The robustness attained with the EPP deployed accommodates increased disturbances as vibration sources degrade over mission life. However, this was not accomplished with minimum cost. EPP isolation provides the necessary attenuation at lower frequencies and RWA isolation provides additional attenuation at higher frequencies. Well after the dual-isolation design approach had been established, enhanced modeling of disturbances, improved understanding of instrument sensitivity to disturbances, and availability of system-level ground-based testing results indicated that either design approach likely would have been sufficient on its own. Flight results now appear to confirm these predictions. The results will be taken into account for the GOES-S, GOES-T, and GOES-U missions.

6. ATTITUDE DETERMINATION AND IRE PERFORMANCE

For attitude determination, GOES-R utilizes the Northrop Grumman Scalable Space Inertial Reference Unit (SSIRU) for the IMU, and the SODERN Hydra with three optical heads for the star tracker. The design includes 2 SSIRUs with 4 gyros each, but only one SSIRU is powered on at a time. The SSIRU was chosen for its high bandwidth and low latency rate output, and for its low-noise characteristics. The 4 gyros are sampled at 200 Hz, and the star tracker optical heads are sampled at 20 Hz. Attitude estimation is performed using a kinematic 6-state extended Kalman filter [23], which combines quaternion outputs from the star tracker with angular rate measurements from the SSIRU to produce a 3-state attitude error estimate and 3-state gyro bias error estimate. As with previous GOES satellites, accurate attitude and rate estimates are critical to INR performance as they are used in the ground-based motion reconstruction and compensation. For GOES-R, rate estimates are also used for real-time ABI mirror control [7][8]. Two samples of 200 Hz gyro data are collected, filtered, bias-corrected and converted to 3-axis rate data before sending to ABI at 100 Hz.

In the GOES-R attitude determination implementation, the gyro and star tracker measurements are synchronized with the spacecraft control frame to provide the most accurate attitude estimate possible. The IRE requirements specify how much error can be accumulated when integrating SSIRU gyro rates. As shown in Table 1, IRE requirements are specified over different time windows from 1 to 900 seconds. The 1 second window is driven by gyro angle white noise (AWN), whereas the other windows are driven by a combination of AWN, bias stability, Kalman filter bias estimation, and alignment stability.

6.1 Attitude Determination Performance

An exact measure of attitude determination performance is difficult, due to the lack of a “truth” model. However, examination of the various attitude determination telemetries lends insight into whether the

analytical predictions are accurate, and also makes possible direct verification of specific elements. In order to evaluate overall attitude determination performance, the 100 Hz IMU data can be used to propagate the attitude from an initial quaternion. Comparison of this propagated quaternion to the Kalman filter attitude estimate provides some understanding of the performance for the gyros, the star tracker, and the Kalman filter itself. While this propagated quaternion can hardly be considered the true vehicle attitude, comparing it to the Kalman filter attitude estimate captures relative misalignments between the star tracker optical heads and the gyros. It also provides a reasonable estimate of both the fast and slow dynamic attitude knowledge errors. Fig. 18 presents the results of this computation over the period of one orbit, along with +/- 15 µrad limits about a 10 minute running average. The results show the 30 µrad dynamic attitude knowledge requirement is met with ~50% margin. It also shows that for this time period the slow dynamic requirement of 45 µrad is also met. This latter requirement is more problematic for winter months where the star tracker radiator is exposed to the sun, and diurnal temperature fluctuations induce small alignment shifts. This will be discussed further below.

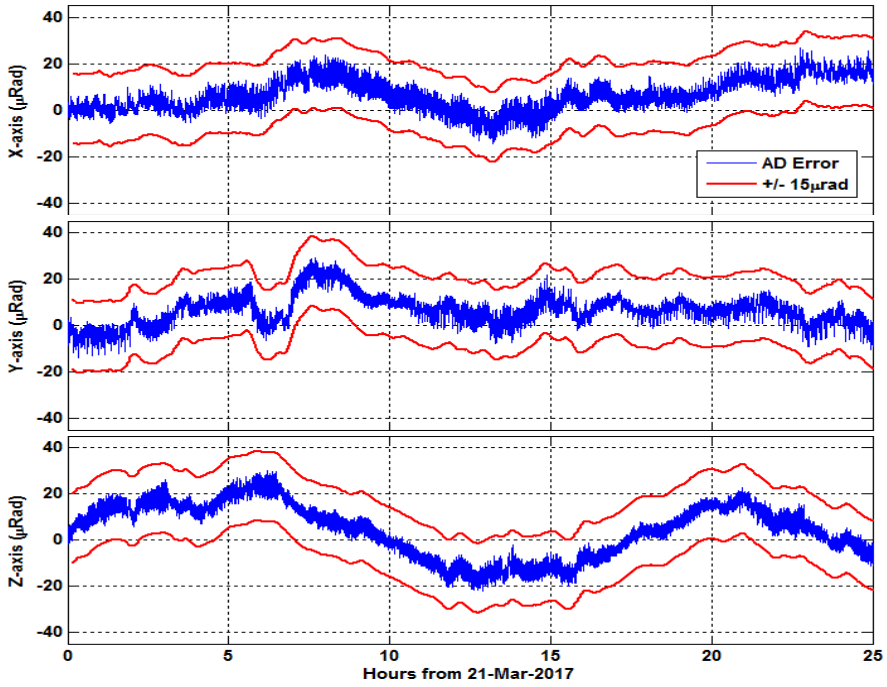

Fig. 18. *Difference between Kalman Filter Attitude Estimate and Propagated 100 Hz Rate Data over One Orbit*

6.2 Integrated Rate Error Performance

Like attitude determination performance, IRE is difficult to estimate without a known truth model for the windows of interest. Acceptance testing of the SSIRUs included granite block testing over a 24 hour period, which showed SSIRU's installed on GOES-16 comply with the IRE requirements. The results for the primary IMU are shown in Table 5. For assessment of flight data, the same technique discussed in the previous section can be used to bound the IRE performance. Fig. 19 shows 300- and 900-sec IRE windows for a 3-hour quiet period of spacecraft operations. The quiet period includes a demonstration of tight thermal control for both the IMU and the star tracker mounting interfaces. Instruments were operating in their nominal scanning and data collection modes. The 900-sec window is clearly compliant, but the 300-sec window is right at the requirement limit using this conservative analysis technique. We can conclude that the 300-sec IRE is likely compliant as well because of the conservatism of this analysis. The 1-sec IRE window can be assessed by processing the 100 Hz data and looking at the high frequency PSD behavior. This approach contains disturbances that degrade the AWN estimate. Nevertheless, AWN computed this way is 0.00243 arcsec/rt-Hz, which is compliant with the IRE-derived requirement of 0.00245 arcsec/rt-Hz. The 30-sec IRE windows are more difficult to assess from flight data. The data set needed for this assessment would require the spacecraft to disable attitude control, gimbal control, and instrument operations for some period of time while collecting high rate gyro data and star

tracker attitude data. For obvious reasons, the program declined to collect this data set. It is reasonable to conclude that the pre-launch data collection discussed in [1][2] sufficiently verifies the 30-sec IRE requirements. Even though it is difficult to say unequivocally the flight data demonstrate IRE requirement compliance, the flight results are consistent with the pre-launch test data and analysis.

Table 5: *IRE Performance Predictions based upon 24-hour Granite Block Test Data*

Axis	1 sec IRE			30 sec IRE			300 sec IRE			900 sec IRE		
	Req	Max	Margin	Req	Max	Margin	Req	Max	Margin	Req	Max	Margin
X	1	0.76	24%	2	0.87	57%	7	1.61	77%	18.5	2.47	87
Y	1	0.75	25%	2	0.88	56%	7	1.78	75%	18.5	2.6	86
Z	1.5	0.83	44%	2.5	0.96	62%	7	1.75	75%	18.5	2.71	85

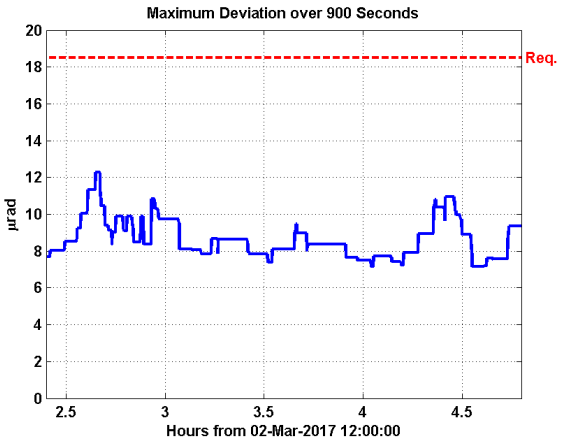

Fig. 19a. *Maximum Deviation over 900 sec*

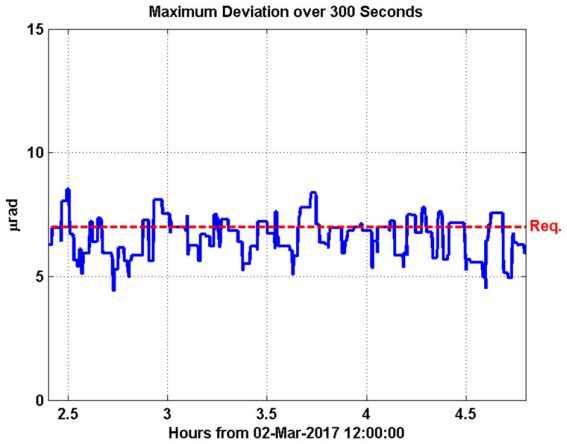

Fig. 19b. *Maximum Deviation over 300 sec*

6.3 Gyro Single Event Upsets

Examination of 200 Hz gyro data revealed an occasional spike in a single gyro channel. Fig. 20 shows an example with a Gyro B rate spike of ~600 micro-rad/sec. These spikes are caused by high energy particles interacting with the gyro control electronics, which cause the gyro angle to jump for a single 200 Hz sample. Back-differencing the gyro angle output results in the rate doublet shown. The transients are too small and too brief to affect the spacecraft attitude determination. However, ABI uses this data unfiltered for mirror control, and these spikes result in degraded imaging. Approximately 40 of these spikes are observed per day, evenly distributed among the 4 gyros. The impacts are significant enough that a FSW patch has been developed to edit out gyro angle spikes above a specified threshold.

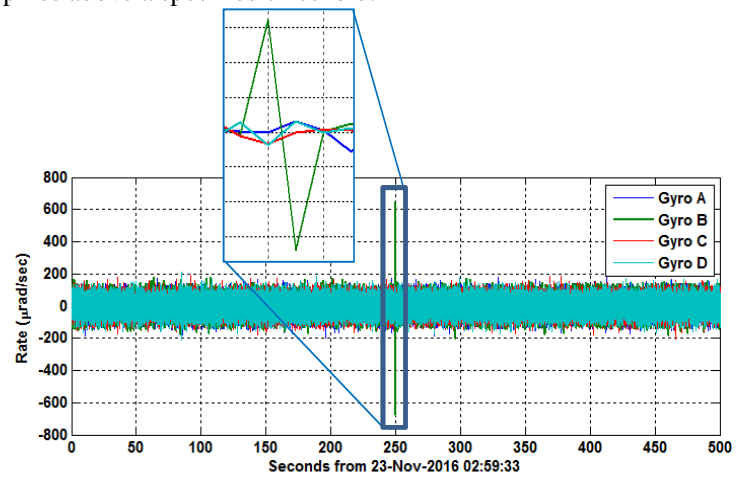

Fig. 20. *Example Gyro Single Event Transient Observed in 200Hz Data*

6.4 Star Tracker Performance

The three-head star tracker is used for attitude measurements, with two heads operating continuously and one serving as a cold spare. GOES-R implements the Hydra capability to synchronize star measurements with an externally provided 20 Hz reference signal. Star measurements from the multiple heads are combined within the star tracker software by rotating the measurements into a common reference frame and applying a QUEST optimization [24] to produce a "fused" attitude estimate from the optical heads [25]. The fused solution also corrects for alignment errors between optical heads. An alignment Kalman filter continuously updates the inter-head alignment transformation to correct for variation of the secondary optical heads with respect to the primary optical head. Fig. 21 shows the star tracker measurement residuals and number of tracked stars for a 96 hour period, the first 42 hours of which all three OH's were operating. As shown the star tracker is usually able to routinely track 15 stars on each head simultaneously at 20 Hz. Measurement residuals are 21.5 µrad with two optical heads operating, and 18.9 µrad with three optical heads. The observed performance is slightly better than pre-launch predictions presented in [1][2], and indicate excellent star tracker performance.

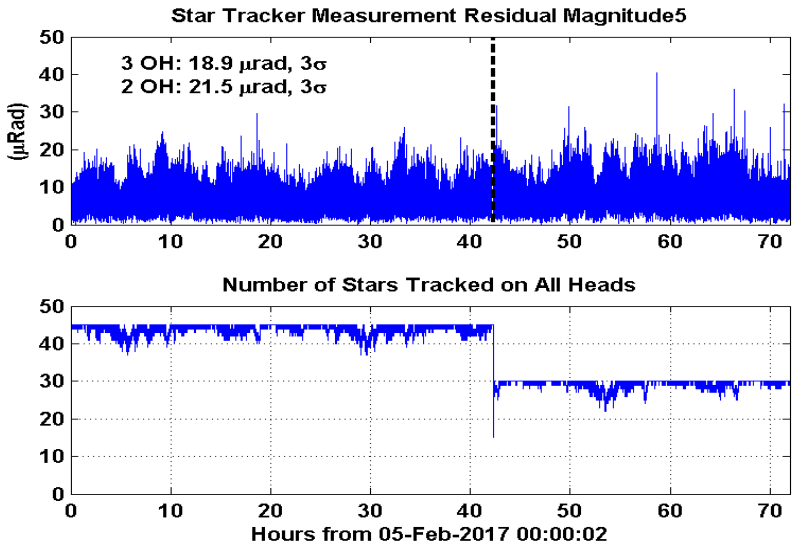

Fig. 21. *Star Tracker performance for GOES-R*

6.5 Star Tracker and IMU Alignment Calibrations

The 6-state Kalman filter does not include any estimation of alignment errors between the SSIRU and the star tracker, nor does it include gyro scale factor estimates. Instead, a post-launch calibration sequence was performed to estimate gyro to star tracker alignments as well as gyro scale factor errors (SFE). The calibration maneuvers consisted of 19 deg slews about each gyro axis. Propagated attitude from the gyros and star tracker quaternion solutions were collected at 1 Hz. Table 6 shows the estimated alignment errors and gyro SFE from the calibration sequence, as well as pre-launch gyro SFE. The calibration sequence was repeated after the derived alignment and gyro SFE corrections were uplinked to the spacecraft. Table 6 also includes alignment error and SFE for the updated parameter set, providing a good measure of the calibration accuracy. The post-calibration measurements indicate the alignment calibration requirement of 200 micro-radians (gyro axes to star tracker axes) and the gyro scale factor error requirement of 2250 ppm, 3σ, are both met with margin.

Table 6: *GOES-R Alignment and Gyro Scale Factor Calibration Performance*

Gyro Alignment and Scale Factor Calibration Results					
	Misalignments (µRad)		Scale Factor Errors (ppm)		
	Pre-Cal	Post-Cal	Gyro ATP	Pre-Cal	Post-Cal
Gyro A	181	79	571	891	0.3
Gyro B	177	156	202	422	36

Gyro C	98	75	754	1173	53
Gyro D	335	118	112	188	52

Fig. 22 shows the time histories comparing the star tracker quaternion with the propagated gyro attitude for both the pre-calibration and the post-calibration slew sequences. As observed in Fig. 22, the residuals peaked at larger values during the initial slew sequence, indicating that the calibration was successful.

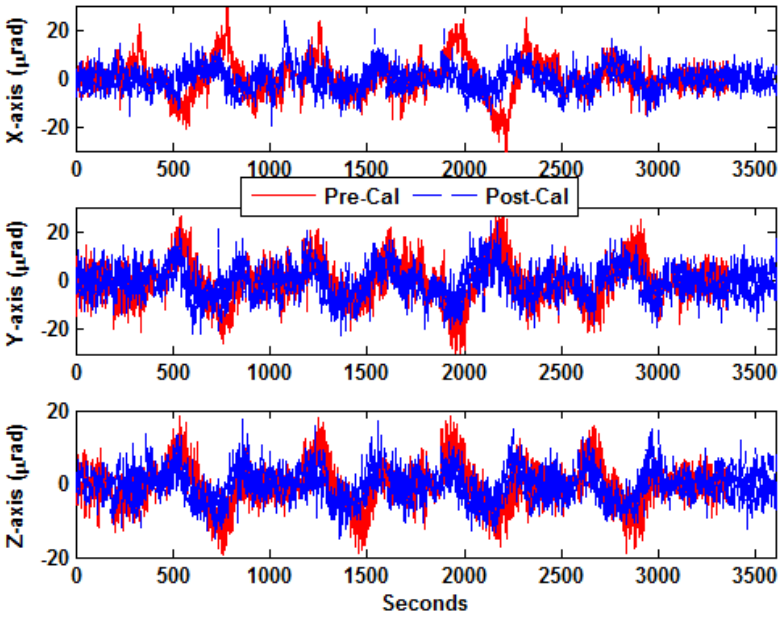

Fig. 22. *Attitude Residuals for Pre and Post IMU-Star Tracker Calibration Slews*

6.6 Star Tracker and IMU Heater Disturbances

Analysis of the attitude telemetry shortly after launch revealed some off-nominal performance in the thermal control system. Most significant was a rate transient in the X-axis that appeared to coincide with IMU mounting interface heater cycling. The rate transients were large enough to cause a response by the attitude control FSW, and a corresponding attitude disturbance. The heater settings were modified to decrease the hysteresis in the thermal control, and to primarily use the heater furthest away from the IMU, which produced the smallest attitude transient. This modification reduced the rate transients such that attitude disturbances were no longer visible in the nominal telemetry. However, closer examination of the 100 Hz attitude rate data revealed that small transients of approximately 10 μrad were still present, and directly correlated to IMU heater cycling. To mitigate this effect a FSW patch has been developed to provide tighter control of the IMU mounting interface temperature, which will reduce the heater-induced transients to less than 1-2 μrad.

In addition to the transients induced by the IMU heater, attitude transients were also found to result from star tracker heater cycling. Whereas the IMU heater transients are mostly observable in the X-axis, the star tracker heater transients are most prominent in the Y-axis. The star tracker heater heater-induced transients are a little more complex to analyze, because the most directly observable effect is a corruption of gyro bias estimate. This produces what appears to be a gyro rate, but in reality it is a variation of the gyro bias estimate induced by the star tracker heater. The same FSW patch developed for the IMU heater control will also be deployed for star tracker mounting interface temperature control, with similar performance improvements expected. The transients caused by the star tracker mounting interface heaters will also be reduced to 1-2 μrad.

Fig. 23 shows the IMU and star tracker heater states over 3 hours plotted above the X and Y-axis attitude motion derived from the high-rate IMU telemetry. The attitude transients are clearly correlated to the heater activity. As observed in Fig. 23, the IMU heater activity shows up almost exclusively in the X-axis, whereas the star tracker heater activity show up mostly in the Y-axis, with some effect also noticeable in the X-axis.

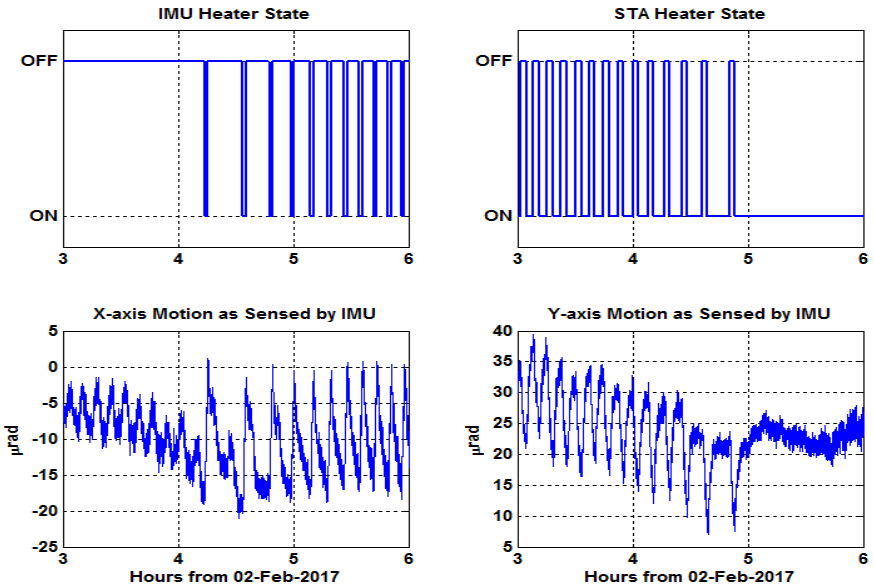

Fig. 23. *Attitude Rate Transients Induced by IMU and Star Tracker Heater Cycling*

6.7 Diurnal Alignment Perturbations

After achieving GEO and transitioning to nadir-pointed operations, the star tracker temperatures were observed to be significantly different than pre-launch predictions. The star tracker thermal interface was designed to be cold-biased, such that the mounting interface would be maintained at a constant temperature by active heater control. Instead, large diurnal swings in temperature were observed, as shown in Fig. 24. For these two days of GEO operations, the star tracker mounting bracket peaked at 37 deg C from a control temperature of 5 deg C. Analysis has shown that the star tracker bracket alignment varies with temperature relative to the IMU. The alignment variation for this thermal profile is ~200 µrad, which violates the 54 µrad diurnal alignment variation requirement. For the period between the autumnal equinox and vernal equinox, the star tracker thermal radiator is exposed to the sun and this diurnal temperature variation is now expected to occur. For the other half of the year, the star tracker radiator is not exposed to the sun and the temperatures are well controlled.

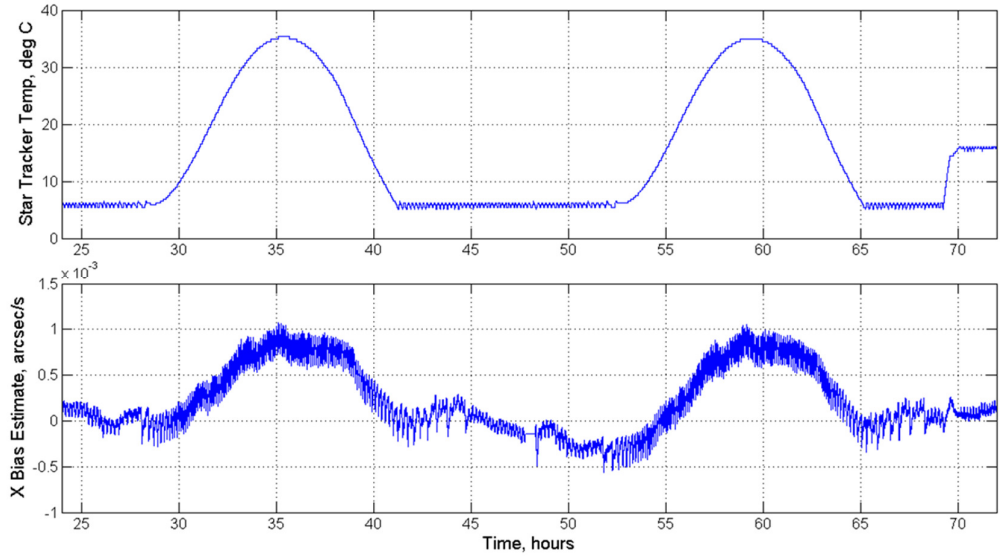

Fig. 24. *Star Tracker Mount Diurnal Temperature Variation Impacts to Gyro Bias Estimation*

Although the star tracker itself can operate at these peak temperatures, the diurnal bracket alignment variation causes a performance issue evident in the lower plot of Fig. 24, which shows the X-axis gyro bias estimate for

this period. There is a clear correlation between the star tracker baseplate temperature and the gyro bias estimate. Obviously, the gyro biases are not directly affected by star tracker bracket temperature. Because the Kalman filter only has 6-states, it erroneously attributes alignment variation between the star tracker and the IMU to variation in the gyro bias. This variation degrades the accuracy of the spacecraft attitude estimate.

Because of the slow alignment variation and because ABI internally estimates attitude based upon periodic star sightings, this diurnal behavior does not significantly impact ABI observations. However, the GLM instrument depends upon having small diurnal attitude variations. The investigation of potential mitigations for GLM is ongoing. For GOES-16, the star trackers can be operated at an elevated temperature throughout the winter months, thereby limiting the peak-to-peak thermal variation. For the GOES-S, T, and U vehicles, thermal design modifications are underway to improve thermal stability of the star tracker mounting interface.

7. ORBIT DETERMINATION PERFORMANCE

Use of a GPS receiver on a spacecraft is desirable for three main reason: 1) improved positon, velocity and timing (PVT) accuracy, 2) reduced ground support demands, and 3) increased automation through availability of PVT directly to FSW. The GOES-R GN&C component suite includes the upgraded Viceroy-4 GPS Receiver (GPSR) from General Dynamics coupled with a GPS antenna designed by Lockheed Martin. The Viceroy-4 was developed specifically for the GOES-R program, and the antenna design was tailored for operations in a Geosynchronous Earth Orbit (GEO). The new GPSR design and custom GEO antenna design enable onboard autonomous navigation, which is a critical enabling technology for this mission.

A GPS receiver at GEO altitude (~35,786 km) is 15,000 km farther away from Earth than the GPS constellation. Satellites comprising the GPS constellation are designed to transmit signals towards Earth. Therefore, a GEO spacecraft such as GOES-R must point its GPS receive antenna towards nadir to receive the GPS signals that leak around the Earth, as shown in Fig. 25.

A GPS receiver performs optimally when it tracks 4 or more GPS Satellites. Analysis shows that this cannot be achieved at GEO when only the GPS main lobe signals are used [11][13]. Because GPS side lobe signals are inherently weak, and because side lobe free space path loss in GEO can be more than 10 dB compared with main lobe free space loss in low Earth orbit, tracking GPS at GEO is very challenging. A GPS receiver attempting to exploit side lobe information must have the dynamic range to distinguish a low power signal from noise, while not saturating with a high-power signal present [13]. The Viceroy-4 GPSR was designed and tuned in order to facilitate tracking the extremely weak GPS signals at GEO (on the order of 10^{-18} W).

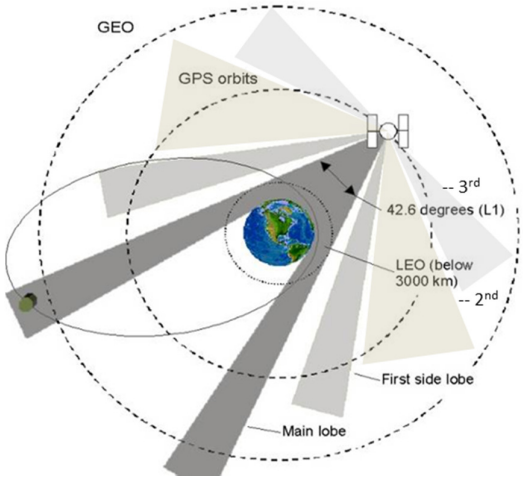

Fig. 25. *GOES-R Geometry Depiction in Orbital Slot*

On GOES-16, the GPSR was powered on shortly after orbit-raising was complete. The observed performance allowed it to be used as the primary source of orbit data after only a few days of operation. Only a brief summary of the GOES-16 performance is presented here; more detailed performance results are presented in

[10]. As shown in Fig. 26 the average carrier-to-noise density (C/N0) is approximately 31.5 dB-Hz, which is about 3 dB higher than the performance specifications. This high C/N0 average allows more contiguous tracking of GPS satellites, improving the navigation solution. The minimum, maximum, and average number of tracked GPS satellites for the same 2 month period is shown in Fig. 26. The GPSR tracks between 11 and 12 GPS satellites on average, with no outages. The GPS satellite tracking performance is much better than pre-launch simulations predicted, although those simulations used very conservative assumptions on antenna gain and various signal losses. Other systems that have employed GPS at GEO only used the GPS satellites' main lobe. They average less than 4 GPS satellites tracked and suffer significant outage periods. The ability to use the side lobes dramatically improves the availability of GPS signals as well as the achievable solution accuracy.

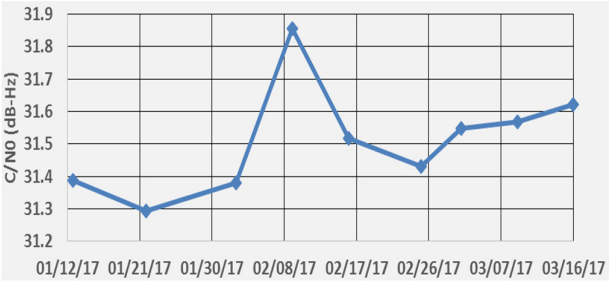

Fig. 26a. *GOES-16 GPSR Carrier-to-Noise Density Trend*

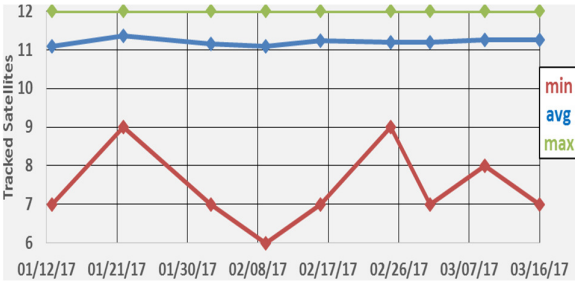

Fig. 26b. *GOES-16 GPSR Tracked Satellites Trending*

The GOES-R orbit determination accuracy requirements are shown above in Table 1, and observed GOES-16 performance results for a 50 hour representative period are summarized in Table 7. The period includes multiple MA events and an NSSK maneuver. The error assessment was derived from post-processing raw data from an external Kalman filter and data from National Geospatial-Intelligence Agency's (NGA) precise GPS ephemeris. The results demonstrate compliance with the orbit knowledge performance requirements. Details of the analysis approach and a comprehensive description of the results are presented in [10].

Table 7: Accuracy Enumeration from 50 hour Data Sample, position variance 3m

99.7% = mean +/- 3σ	Position (m)			Velocity (cm/s)		
	Radial	In-Track	Cross-Track	Radial	In-Track	Cross-Track
Mean	2.6	0.7	-0.4	0.019	0.001	-0.023
3σ	20.3	13	7.3	0.4	0.28	0.69
Upper Bound	22.9	13.7	6.9	0.419	0.281	0.667
Lower Bound	-17.7	-12.3	-7.7	-0.381	-0.279	-0.713

Maintaining accurate orbit knowledge through thruster events is critical for providing the operate-through capability. The position and velocity performance for a representative NSSK maneuver are shown in Fig. 27. The average variance of ~3m for the precise external filter is shown by the dotted line on the position error plot. The delta-V for the maneuver was approximately 2 cm/s in the south direction, as can be seen in the position and velocity cross-track error signature at the 7-hour time mark. The maneuver lasted for 11 minutes. The GOES-R implementation does not include any feedforward of the delta-V maneuver to the GPSR, other than to increase the covariance in the GPSR Kalman filter at the start of the maneuver. The GPSR is able to track the maneuver well within requirements, with the most significant impact being an increased cross-track velocity error that required nearly an hour to return back to pre-maneuver levels. However, the observed performance in this example is still ~3X better than the 6 cm/s requirement. This performance is possible because of the excellent GPS constellation tracking performance throughout the maneuvers. No GPS constellation tracking outages have occurred during any maneuvers to date.

The GOES-16 GPSR performance meets all performance requirements, tracking up to 12 satellites with no outages, and achieving excellent carrier-to-noise density (C/N0). The performance results show the practically of this approach. Future GEO satellites will benefit from improved orbit knowledge accuracy and reduced ground support requirements.

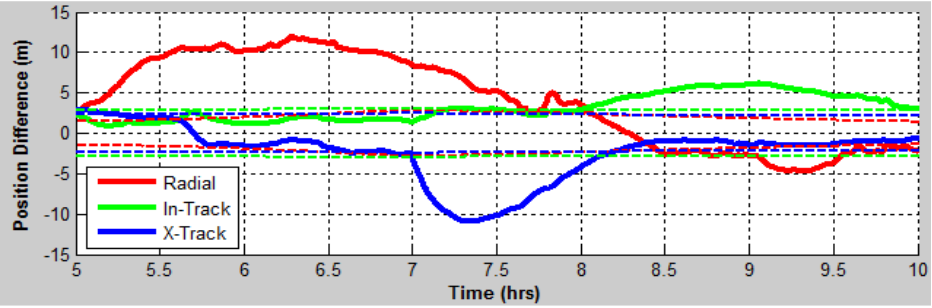

Fig. 27a. *GOES-16 GPSR Position Error during NSSK Maneuver as Differenced with Ground EKF Solution*

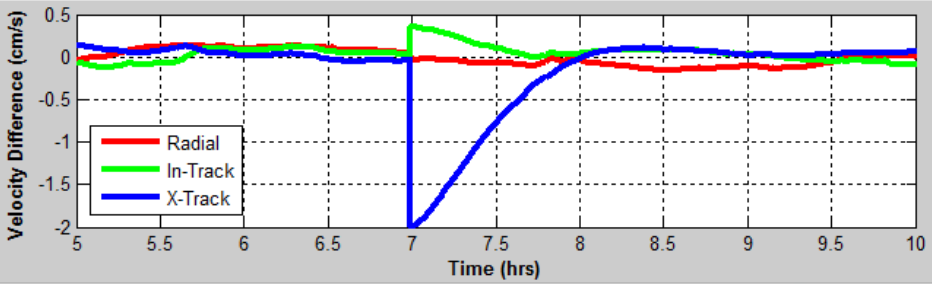

Fig. 27b. *GOES-16 GPSR Velocity during NSSK Maneuver Error as Differenced with Ground EKF Solution*

8. CONCLUSION

The on-orbit commissioning of the GOES-16 spacecraft has ushered in the next generation of earth, solar and space weather observations with quantum improvements in spectral, spatial and temporal resolution. The realization of this performance imposed demanding requirements on the GN&C subsystem, which were achieved through the use of several key enabling technologies:

- The LTR thruster development enables "operate-through" capability during MA, NSSK, and EWSK maneuvers, which in turn provides unprecedented availability of Earth-observation data.
- The attitude and articulation control law implementations include several unique feedforward and timing features to meet stringent pointing and pointing stability requirements, even in the presence of disturbances from MA, NSSK, and EWSK maneuvers, and instrument steering mirror control.
- Active Vibration Damping mitigates flexible body modes, including solar array and magnetometer boom dynamics.
- Dual RWA and EPP isolation satisfies the jitter and instrument interface acceleration requirements across a broad spectrum 0-512 Hz.
- The attitude determination design meets challenging requirements by implementing high-performance star trackers and IMUs co-located with the instruments on a stable optical bench. The synchronized, high-rate, low-latency gyro data implementation is key to meeting the stringent INR requirements.
- GOES-R implements the first use of civilian frequency GPS receiver at GEO, providing a dramatic step forward in autonomous orbit determination performance. This greatly simplifies mission operations by eliminating the need for ranging, daily ephemeris uploads, and maneuver recovery.

As shown in this paper, the on-orbit performance of the GOES-16 satisfies the challenging mission objectives of the next generation GEO Earth-observation satellites.

9. ACKNOWLEDGEMENTS

This work was performed at Lockheed Martin Space Systems, under NASA contract NNG09HR00C, and at the National Aeronautics and Space Administration Goddard Space Flight Center. The authors gratefully acknowledge the many individuals who contributed in various ways through GOES-R program workshops and reviews, and helped developed a better understanding between instrument operations and spacecraft

performance. The resulting implementation provides a dramatic increase in Earth and Solar weather monitoring capabilities.

10. REFERENCES

[1] J. Chapel, D. Stancliffe, T. Bevacqua, S. Winkler, B. Clapp, T. Rood, D. Gaylor, D. Freesland, A. Krimchansky, "Guidance, Navigation, and Control Performance for the GOES-R Spacecraft," Proceedings of the 9th International ESA Conference on Guidance, Navigation & Control Systems, Oporto, Portugal, Jun 2014.

[2] J. Chapel, D. Stancliffe, T. Bevacqua, S. Winkler, B. Clapp, T. Rood, D. Gaylor, D. Freesland, A. Krimchansky, "Guidance, Navigation, and Control Performance for the GOES-R Spacecraft," CEAS Space Journal, DOI 10.1007/s12567-015-0077-1, March 2015.

[3] T. J. Schmit, Jun Li, Jinlong Li, W. F. Feltz, J. J. Gurka, M. D. Goldberg, K. J. Schrab, "The GOES-R Advanced Baseline Imager and the Continuation of Current Sounder Products," J. Appl. Meteor. Climatol., 47, 2696–2711.

[4] D. Freesland, D. Chu, A. Reth, A. Krimchansky, M. Donnelly, G. Comeyne, "Advancing the Next Generation GOES-R Operational Availability," Proceedings of the 2005 AAS Guidance and Control Conference, Breckenridge, CO, Feb 2005.

[5] GOES-R Functional and Performance Specification (F&PS), 417-R-PSPEC-0014, Version 2.13, November 17, 2010.

[6] A. A. Kamel, "GOES Image Navigation and Registration System," In GOES-8 and Beyond, Edward R. Washwell, Editor, Proc. SPIE 2812, pp 766-776.

[7] D. Igli, V. Virgilio and K Grounder, 2009, "Image Navigation and Registration for GOES-R Advanced Baseline Imager," Proceedings of the 2009 AAS G&C Conference, Breckenridge, CO, Feb 2009.

[8] D. Igli, 2013, "GOES-R Advanced Baseline Imager Precise Pointing Control and Image Collection," Proceedings of the 2013 AAS Guidance and Control Conference, Breckenridge, CO, Feb 2013.

[9] R. L. Farrenkopf, "Analytic Steady-State Accuracy Solutions for Two Common Spacecraft Attitude Estimators," Journal of Guidance, Control, and Dynamics, Vol. 1, No. 4 (1978), pp. 282-284.

[10] S. Winkler, G. Ramsey, C. Frey, J. Chapel, D. Chu, D. Freesland, A. Krimchansky, M. Concha, "GPS Receiver On-Orbit Performance for the GOES-R Spacecraft," Proceedings of the 10th International ESA Conference on Guidance, Navigation & Control Systems, Salzburg, Austria, Jun 2017.

[11] S. Winkler, C. Voboril, R. Hart, M. King, "GOES-R Use of GPS at GEO (Viceroy-4)," Proceedings of the 2013 AAS Guidance and Control Conference, Breckenridge, CO, Feb 2013.

[12] K. Larson, D. Gaylor, S. Winkler, "Worst-Case GPS Constellation for Testing Navigation at Geosynchronous Orbit for GOES-R," Proceedings of the 2013 AAS Guidance and Control Conference, Breckenridge, CO, Feb 2013.

[13] L. Barker, "GPS Beyond LEO: Signal Environment System Design Considerations," Proceedings of the 2008 AAS Guidance and Control Conference, Breckenridge, CO, Feb 2008.

[14] L. P. Davis, D. R. Carter, T. T. Hyde, "Second-Generation Hybrid D-Strut," Proc. SPIE 2445, Smart Structures and Materials 1995: Passive Damping, 161, May 1995.

[15] D. Freesland, D. Carter, J. Chapel, B. Clapp, J. Howat, and A. Krimchansky, "GOES-R Dual Isolation," Proceedings of the 2015 AAS Guidance and Control Conference, Breckenridge, CO, Feb 2015.

[16] D. Carter, B. Clapp, D. Early, D. Freesland, J. Chapel, R. Bailey, A. Krimchansky, "GOES-16 On-Orbit Dual Isolation Performance Characterization Results," Proceedings of the 10th International ESA Conference on Guidance, Navigation & Control Systems, Salzburg, Austria, Jun 2017.

[17] C. D. Johnson, J. M. Howat, P. S. Wilke, "Vibration Isolation System and Method," U.S. Patent 20140084527A1, Moog, Inc., Publication Date Mar 27, 2014.

[18] D. Freesland, A. Reth, A. Krimchansky, M. Donnelly, Tim Walsh, "Improving Attitude Stability Performance on GOES-R Using PIFT," Proceedings of the 2007 AAS Guidance and Control Conference, Breckenridge, CO, Feb 2007.

[19] B. R. Clapp, H. J. Weigl, N. E. Goodzeit, D. R. Carter, and T. J. Rood, "GOES-R Active Vibration Damping Controller Design, Implementation, and On-Orbit Performance," Proceedings of the 10th International ESA Conference on Guidance, Navigation & Control Systems, Salzburg, Austria, Jun 2017.

[20] N. E. Goodzeit, H. J. Weigl, "Active Vibration Damping (AVD) System for Precision Pointing Spacecraft," U.S. Patent WO2008136881A1, Lockheed Martin, Publication Date Nov 13, 2008.

[21] J. Chapel, E. Schmitz, W. Sidney, M. Johnson, P. Good, J. Wynn, T. Bayer, "Attitude Control Performance for MRO Aerobraking and the Initial Science Phase," Proceedings of the 2007 AAS Guidance and Control Conference, Breckenridge, CO, Feb 2007.

[22] F. L. Markley, R. G. Reynolds, F. X. Liu, K. L. Lebsock, "Maximum Torque and Momentum Envelopes for Reaction-Wheel Arrays." Journal of Guidance, Control, and Dynamics. Vol. 33, No. 5. September–October 2010

[23] E. J. Lefferts, F. L. Markley, and M. D. Shuster, "Kalman Filtering for Spacecraft Attitude Estimation," Journal of Guidance, Sep-Oct, 1982, Vol 5, No 5, p. 417.

[24] Shuster, M. D., Kalman Filtering of Spacecraft Attitude and the QUEST Model. Journal of the Astronautical Sciences, 38, 377-393.

[25] D. Piot, L. Oddos-Marcel, B. Gelin, A. Thieuw, P. Genty, P. Martinez, S. Airey, "HYDRA Star Tracker On-board SPOT-6," Proceedings of the 2013 AAS Guidance and Control Conference, Breckenridge, CO, Feb 20013.